Adenylyl cyclase AC8 directly controls its micro-environment by recruiting the actin cytoskeleton in a cholesterol-rich milieu

Laura J. Ayling[1], Stephen J. Briddon[2], Michelle L. Halls[1], Gerald R. V. Hammond[1], Luis Vaca[3], Jonathan Pacheco[3], Stephen J. Hill[2] and Dermot M. F. Cooper[1,*]

[1]Department of Pharmacology, University of Cambridge, Tennis Court Road, Cambridge, CB2 1PD, UK
[2]Institute of Cell Signalling, School of Biomedical Sciences, University of Nottingham, Queens Medical Centre, Nottingham, NG7 2UH, UK
[3]Departamento de Biología Celular, Instituto de Fisiología Celular, Universidad Nacional Autónoma de México, Ciudad Universitaria, 04510, México
*Author for correspondence (dmfc2@cam.ac.uk)

Accepted 26 September 2011
Journal of Cell Science 125, 869–886

doi: 10.1242/jcs.091090

Summary

The central and pervasive influence of cAMP on cellular functions underscores the value of stringent control of the organization of adenylyl cyclases (ACs) in the plasma membrane. Biochemical data suggest that ACs reside in membrane rafts and could compartmentalize intermediary scaffolding proteins and associated regulatory elements. However, little is known about the organization or regulation of the dynamic behaviour of ACs in a cellular context. The present study examines these issues, using confocal image analysis of various AC8 constructs, combined with fluorescence recovery after photobleaching and fluorescence correlation spectroscopy. These studies reveal that AC8, through its N-terminus, enhances the cortical actin signal at the plasma membrane; an interaction that was confirmed by GST pull-down and immunoprecipitation experiments. AC8 also associates dynamically with lipid rafts; the direct association of AC8 with sterols was confirmed in Förster resonance energy transfer experiments. Disruption of the actin cytoskeleton and lipid rafts indicates that AC8 tracks along the cytoskeleton in a cholesterol-enriched domain, and the cAMP that it produces contributes to sculpting the actin cytoskeleton. Thus, an adenylyl cyclase is shown not just to act as a scaffold, but also to actively orchestrate its own micro-environment, by associating with the cytoskeleton and controlling the association by producing cAMP, to yield a highly organized signalling hub.

Key words: Adenylyl cyclase, cAMP, Cytoskeleton, Cholesterol, FRAP, Rafts

Introduction

The numerous cellular effects modulated by the ubiquitous second messenger cAMP, underscores the need for stringent control of its spatial and temporal reach. Substantial evidence has established that cAMP 'microdomains' exist, which facilitate discrimination in signal propagation (Bacskai et al., 1993; Buxton and Brunton, 1983; Iancu et al., 2008; Jurevicius and Fischmeister, 1996; Rich et al., 2000; Zaccolo and Pozzan, 2002). These microdomains are partially achieved by scaffolded phosphodiesterases (PDEs), which, by degrading cAMP at specific locations, limit its intracellular diffusion (Lynch et al., 2007; Nikolaev et al., 2006; Willoughby et al., 2006). However, simple limitations on the diffusion of cAMP only partially explain the discrete responses to this second messenger. Organization of the immediate downstream targets of cAMP, namely protein kinase A (PKA), exchange protein activated by cAMP (EPAC) and cyclic nucleotide-gated (CNG) channels, offers an additional level of control. However, recent studies on the binding by adenylyl cyclases (ACs) of various regulatory proteins such as PKA, A-kinase anchoring proteins (AKAPs) (Bauman et al., 2006; Efendiev et al., 2010; Willoughby et al., 2010b), protein phosphatase 2A (PP2A) (Crossthwaite et al., 2006), snapin (Chou et al., 2004) and phosphodiesterases (PDEs) (Halls and Cooper, 2010) indicate that ACs can to a large extent dictate their micro-environmental milieu. Consequently, the placement and compartmentalization of ACs might provide a primary level of organization of cAMP signalling cascades.

Considerable evidence suggests that ACs exploit the heterogeneity of plasma membranes (PM), represented by the existence of so-called 'lipid rafts'. ACs that are regulated by Ca^{2+} are targeted to these domains, whereas Ca^{2+}-insensitive ACs are excluded (Cooper and Crossthwaite, 2006). The concept of 'membrane rafts' has evolved considerably over the last decade. These were initially envisaged as rather static regions enriched in closely packed sphingolipids (Schroeder et al., 1995) and sterols, such as cholesterol, with a role in membrane phase behaviour (Brown and London, 2000), trafficking (Gruenberg, 2001) sorting (Hansen et al., 2000) and organization of signalling complexes (Brown and London, 1998; Head et al., 2006). Membrane rafts are increasingly understood to be small (10–200 nm), well dispersed, dynamic and detergent-resistant structures that provide a platform for the establishment of microdomains, which can be quite transient (Hancock and Parton, 2005; Lingwood et al., 2008).

An additional major contributor to membrane component organization is the actin cytoskeleton, which acts as a physical barrier by forming a highly reticulated network of filaments beneath the PM. Transient corrals are formed by the association

of actin or actin-binding proteins with raft proteins (Rodgers and Zavzavadjian, 2001), momentarily restricting the diffusion and dispersal of membrane proteins (Sako and Kusumi, 1994; Suzuki et al., 2005). Evidence has already been gathered to suggest that AC5 and/or 6 compartmentalization in rafts depends on the actin cytoskeleton (Head et al., 2006).

The Ca^{2+}-sensitive ACs (AC1, AC8, AC5 and AC6) are a well-documented example of elegant regulatory associations, so that sophisticated architectural devices might be anticipated in their cellular disposition. These ACs are regulated by the ubiquitous process of capacitative Ca^{2+} entry (CCE) (Parekh and Putney, 2005; Cheng et al., 2011) that is triggered by Ca^{2+} store depletion, and are unresponsive to other forms of Ca^{2+} rise (Fagan et al., 1996; Martin et al., 2009; Willoughby and Cooper, 2007). The selective regulation of AC8 by CCE depends upon the residence of AC8 in lipid rafts (Pagano et al., 2009; Smith et al., 2002) in close proximity to store-operated Ca^{2+} entry channels (Willoughby et al., 2010a). However, little is known about the mechanisms behind the establishment and maintenance of this AC8 'microdomain'.

The present study is the first to tackle the role of the actin cytoskeleton and membrane cholesterol in stabilising the integrity of the AC8 microdomain. Although the direct analysis of the physical nature of microdomains and their resident proteins is difficult (because they fall below the resolution of the light microscope) powerful live cell approaches such as fluorescence recovery after photobleaching (FRAP) and fluorescence correlation spectroscopy (FCS) (Kim et al., 2007; Schwille, 2001) can address protein mobility and organization. Using these approaches, we have revealed a dynamic milieu, involving an association between the N-terminus of AC8 and the actin cytoskeleton in a membrane region rich in cholesterol, where the cAMP produced by AC8 modulates the polymerization of actin, thereby exerting control over its own mobility within the membrane.

Results

AC8 enhances the cortical actin signal

Initial experiments examined the distribution of the actin cytoskeleton using phalloidin in untransfected HEK293 cells and cells expressing AC8–HA, AC1–FLAG or AC2–HA. Remarkably, there was a marked difference in the localisation of the actin cytoskeleton when AC8–HA was expressed (Fig. 1A). Filaments of the actin cytoskeleton extended throughout the cytosol in untransfected cells and in cells expressing AC1 or AC2; however, cortical actin at the PM was significantly enhanced when AC8 was expressed (Fig. 1A). Because phalloidin only detects F-actin, the signal from GFP–actin was also examined in cells expressing AC1, AC2 or AC8 (supplementary material Fig. S1A). Highly dispersed G-actin and F-actin were identifiable throughout the cytosol in all cells, however, the GFP–actin signal was enhanced at the PM in cells expressing AC8. Thus the observed redistribution of the cytoskeleton was not the result of the phalloidin staining (supplementary material Fig. S1A). It is not surprising that there are major differences between AC1, AC2 and AC8 given that their N-terminal sequences are quite dissimilar (supplementary material Fig. S1B).

To ensure that this observation was not a function of the HA epitope of AC8, GFP–AC8 was also examined (Fig. 1B). Pearson's coefficient (Rr) was calculated (supplementary material Fig. S2) in order to ascertain the degree of colocalisation between the GFP signal and cellular structural elements. The PM residence of AC8 meant that GFP–AC8 colocalised well with the PM marker wheat germ agglutinin (WGA; $Rr=0.77\pm0.02$; Fig. 1C). Interestingly, GFP–AC8 also consistently colocalised well with the actin cytoskeleton marker phalloidin ($Rr=0.72\pm0.02$), but much less so with the microtubule marker tubulin ($Rr=0.25\pm0.03$; Fig. 1C). Lyn–GFP, a PM-targeted control peptide (Park et al., 2008) (Fig. 1D) also colocalised with WGA ($Rr=0.78\pm0.02$), but less so with phalloidin ($Rr=0.50\pm0.03$; Fig. 1E). Thus the Rr data underline the specificity of AC8 in enhancing the cortical actin signal. In order to analyse the relative distribution of the phalloidin signal in cells expressing GFP–AC8 or Lyn–GFP the ratio of the signal intensity was determined at the PM and in the cytosol ($Ratio_{PM/Cyt}$; supplementary material Fig. S2). $Ratio_{PM/Cyt}$ confirmed that the phalloidin signal was greater at the PM in cells expressing GFP–AC8 (21.2 ± 3.4) than in those expressing Lyn–GFP (6.9 ± 1.1; Fig. 1F). Thus, an association between AC8 and the actin cytoskeleton is strongly suggested.

The enhancement of cortical actin depends on the N-terminus of AC8

To explore the association between AC8 and actin, two mutants were studied: an N-terminally truncated construct, AC8M1, and a catalytically inactive, full-length mutant, AC8 D416N (Fig. 2A). AC8M1 lacks the first 106 amino acids of the N-terminus, a hyper-variable region of ACs that contains several protein binding sites, and thus might be a candidate domain to interact with actin. AC8 D416N was used to elucidate a role for cAMP in actin remodelling; a point mutation at the invariant Mg^{2+}-binding aspartic acid residue (D416) within the C1a catalytic domain renders the enzyme inactive (Howe, 2004; Nadella et al., 2009). All constructs were tagged with GFP at their N-termini (Fig. 2A) and stably expressed (Fig. 2B).

Activity assays were performed in order to define the activity profiles of each construct in vitro (Fig. 2C) and in vivo (Fig. 2D). These experiments confirmed the inactivity of AC8 D416N and demonstrated that GFP–AC8 and GFP–AC8M1 have similar Ca^{2+}-activation profiles in vitro (Fig. 2C), whereas in the intact cell, GFP–AC8 was stimulated 4.0 ± 0.3 fold by 4 mM external Ca^{2+} following triggering of CCE, whereas GFP–AC8M1 required 8 mM external Ca^{2+} for comparable (3.6 ± 0.3 fold) stimulation (Fig. 2D). The reduced responsiveness of AC8M1 to CCE has been attributed to the deletion of an N-terminal calmodulin (CaM) binding domain (residues 34–51), which precludes pre-recruitment of CaM (although additional factors are not excluded) (Gu and Cooper, 1999; Simpson et al., 2006) (Fig. 2D).

The expression and relative distribution of GFP–AC8M1 and GFP–AC8 D416N was determined by confocal image analysis. Although GFP–AC8M1 and GFP–AC8 D416N were both targeted to the PM, the enhancement of cortical actin was only observed in cells expressing GFP–AC8 D416N (Fig. 2E). Indeed the degree of colocalisation between GFP–AC8M1 and phallodin was significantly reduced compared with when GFP–AC8 or GFP–AC8 D416N was expressed (Fig. 2F) and, $Ratio_{PM/Cyt}$ analysis confirmed that the distribution of the actin cytoskeleton was not enhanced at the PM in cells expressing GFP–AC8M1 (Fig. 2G). Thus the redistribution of the cytoskeleton and enhancement of cortical actin by AC8 depends on the N-terminus of AC8; however, a role for cAMP emanating from AC8 is not obvious from these measurements.

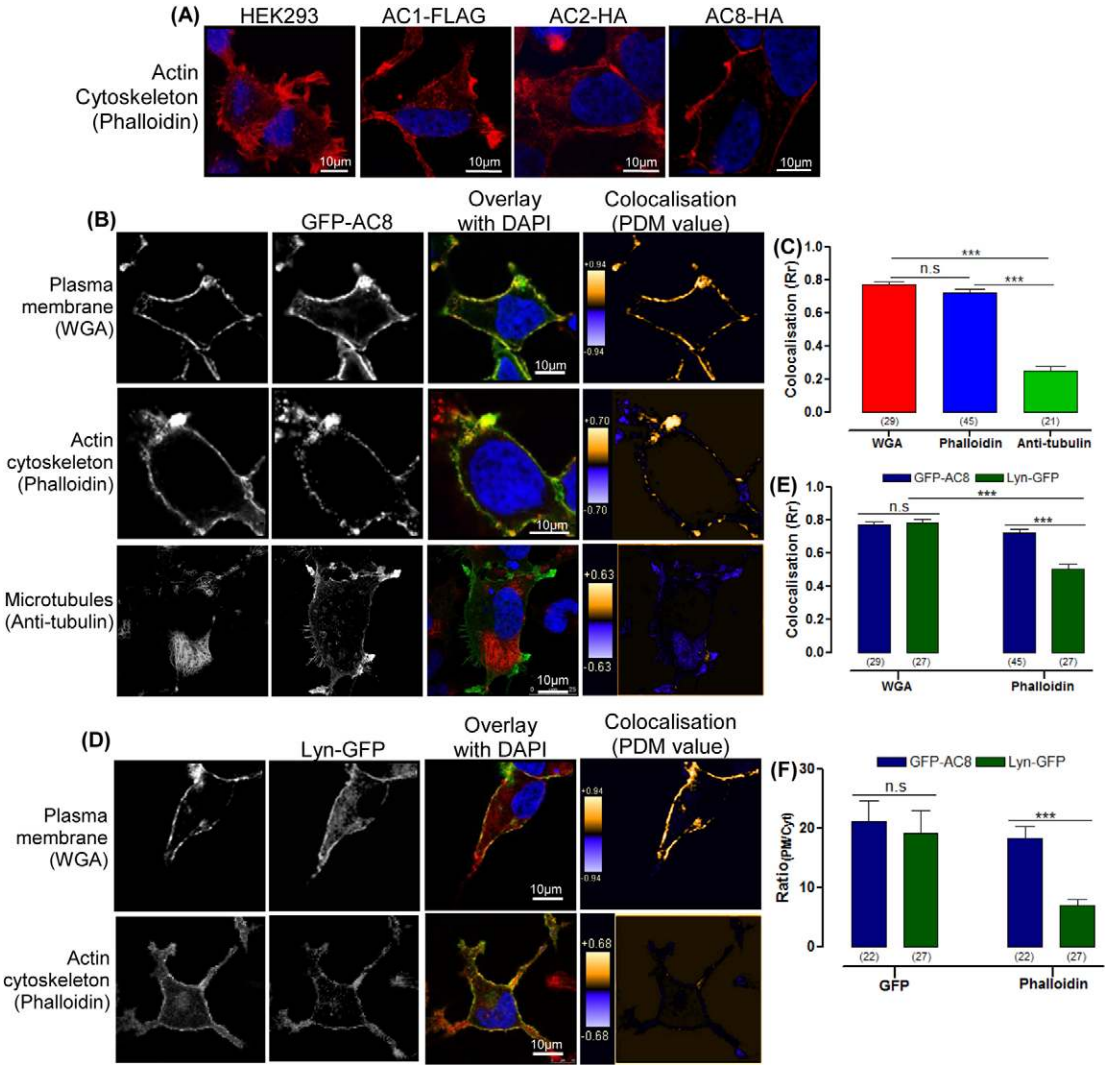

Fig. 1. Expression of AC8 enhances cortical actin. (**A**) HEK293 cells stained with phalloidin, stably expressing AC1–FLAG, AC2–HA or AC8–HA, as determined by cAMP accumulation analysis (data not shown). (**B**) Cells expressing GFP–AC8 stained with WGA, phalloidin or anti-tubulin antibody; graphical representations of PDM values of colocalisation are shown in the right panels. (**C**) Colocalisation (Rr) analysis for B. (**D**) Cells expressing Lyn–GFP stained with WGA or phalloidin are shown in the right panels. (**E**) Colocalisation (Rr) analysis of GFP–AC8 or Lyn-GFP with WGA or phalloidin. (**F**) $Ratio_{PM/Cyt}$ analysis of GFP–AC8, Lyn–GFP and phalloidin.

GST pull-down and co-immunoprecipitation (co-IP) experiments confirm an association between AC8 and actin

In order to investigate biochemically the interaction between AC8 and the actin cytoskeleton, GST pull-down experiments were performed. In the absence of Ca^{2+}, only full-length 8NT (residues 1–179) significantly pulled down actin, compared with the level using unconjugated GST beads (Fig. 3A–C; $n=5$). Interestingly, the separate halves of the N-terminus of AC8 did not pull down actin, suggesting that the N-terminus must be intact and adopt an integrated secondary structure to associate with actin. The interaction between 8NT and actin was lost in the presence 10 μM Ca^{2+} (Fig. 3A–C; $n=5$). The presence of Ca^{2+} allows endogenous CaM to bind to both known CaM binding domains in the 8NT and 8C2b fragments. To further explore the interaction between actin and the N-terminus of AC8, HA co-IP experiments were performed with cell lysates prepared from cells expressing full-length AC8–HA or AC8M1–HA. AC8–HA, but not AC8M1, pulled down actin (Fig. 3D,E; $n=3$). Therefore, both biochemical and single cell confocal experiments indicated that the N-terminus of AC8 associates with the actin cytoskeleton. Furthermore, the AC8–actin interaction is affected by Ca^{2+}–CaM and requires the complete N-terminus.

The distribution and regulation of GFP–AC8 depends on the intact actin cytoskeleton

To explore the functional significance of the AC8–actin interaction in a cellular context, the cytoskeleton was disrupted with latrunculin B (LatB; 2 μM). This pharmacological tool binds to G-actin to produce shorter, thicker stress fibres and thereby promote the complete passive disruption of the actin filaments. Treatment with LatB led to the aggregation and partial internalization (37%) of GFP–AC8 (Fig. 4A–C; supplementary

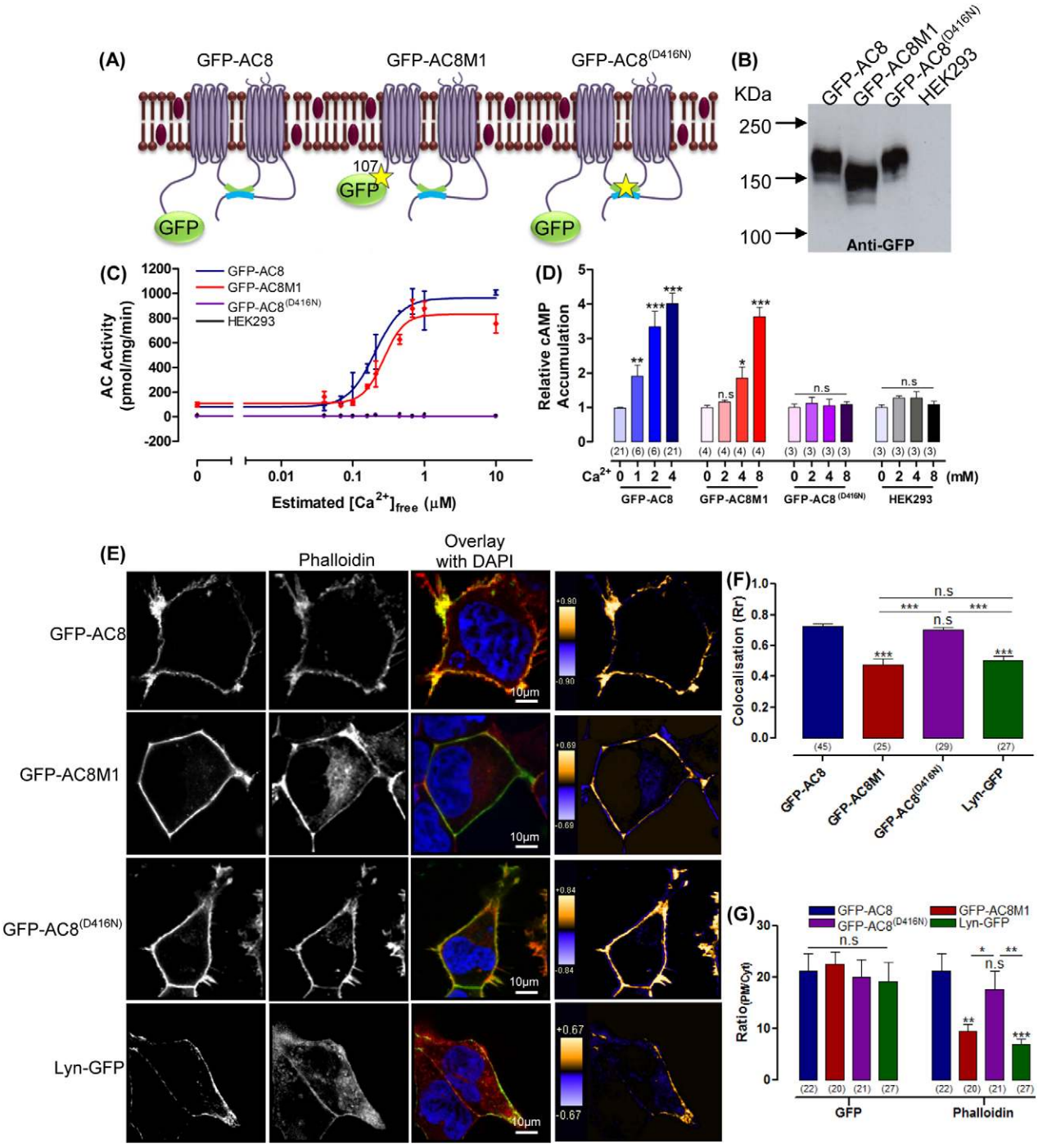

Fig. 2. The N-terminus of AC8 redistributes the actin filaments. (**A**) Representation of GFP–AC8, GFP–AC8M1 and GFP–AC8 D416N (GFP–AC8$^{(D416N)}$). (**B**) Western blot analysis of crude membranes from cells expressing GFP–AC8, GFP–AC8M1 or GFP–AC8 D416N. (**C**) Representative experiment measuring AC activity in membrane expressing GFP–AC8, GFP–AC8M1 or GFP–AC8 D416N in response to Ca^{2+}. (**D**) cAMP accumulation in whole cells expressing GFP–AC8, GFP–AC8M1 or GFP–AC8 D416N in response to CCE. (**E**) Phalloidin-stained cells expressing GFP–AC8, GFP–AC8M1, GFP–AC8 D416N or Lyn-GFP; graphical representations of PDM values of colocalisation are shown in the right panels. (**F**) Colocalisation (Rr) analysis of E. (**G**) Ratio$_{PM/Cyt}$ analysis of E.

material Fig. S3A and Fig. S4) without inducing necrotic or apoptotic characteristics, such as blisters and blebs (supplementary material Fig. S3A), and indeed, several of the AC8 aggregates colocalised with the phalloidin signal of the disrupted cytoskeleton (Fig. 4B). These data indicate that the AC8–actin interaction persists despite cytoskeletal disruption.

The regulation of voltage-gated ion channels (Schubert and Akopian, 2004) and Lck (Chichili and Rodgers, 2007) are both compromised when the actin cytoskeleton is disrupted. In order to investigate whether the intact actin cytoskeleton is essential for regulation of GFP–AC8, activity assays were performed using the Förster resonance energy transfer (FRET)-based cAMP sensor,

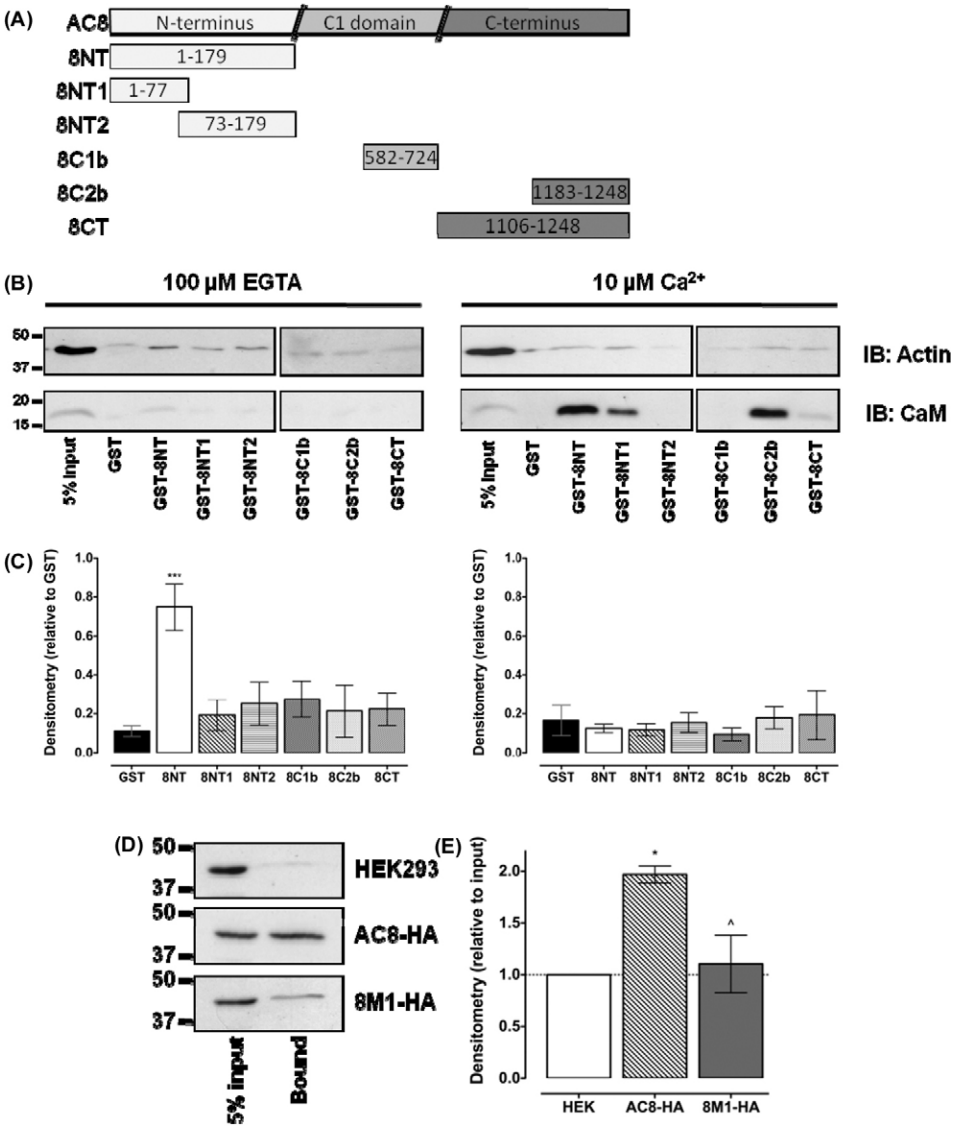

Fig. 3. The N-terminus of AC8 interacts with actin. (**A**) Fragments of AC8. (**B**) GST pull-downs of actin and CaM from cell lysates in the absence (100 µM EGTA) or presence of Ca^{2+} (10 µM), by fragments of AC8. (**C**) Densitometry from B (n=5–6). (**D**) Co-immunoprecipitation of actin in cells expressing AC8–HA or AC8M1–HA. (**E**) Densitometry of D, relative to input and normalized to untransfected HEK293 cells (n=5).

Epac2-camps, in single cells expressing AC8–HA. Untreated cells displayed a robust response to CCE (Fig. 4D). However, disrupting the integrity of the actin cytoskeleton with LatB resulted in the deregulation of GFP–AC8; these cells produced significantly more cAMP under basal conditions (Fig. 4E), but were consequently less stimulated by CCE (Fig. 4F). These Epac2-camps results were mirrored in whole-cell cAMP accumulation experiments (supplementary material Fig. S3B–E). To discount the possibility that the deregulation of AC8 by LatB is due to a diminution or compromising of CCE, CCE was directly assessed by measuring the internal Ca^{2+} concentration ($[Ca^{2+}]_i$) using Fura-2 (supplementary material Fig. S3F). LatB did not significantly alter $[Ca^{2+}]_i$ before or following the induction of CCE (supplementary material Fig. S3G,H). Thus the cytoskeleton is not only essential for the organization of AC8, but it also contributes to the proper regulation of AC8 by CCE. Thus, disrupting the cytoskeleton appears to remove an inhibitory influence that results in a more active enzyme under basal conditions, but, perhaps because of the disruption of an association of the enzyme from the CCE apparatus, the enzyme is less responsive to CCE.

Membrane cholesterol is also essential in the distribution and regulation of AC8

To address the role of membrane rafts in the function and distribution of AC8, rafts were disrupted using methyl-β-cyclodextrin (MβCD) or sphingomyelinase (SMase). MβCD is a chelator of cholesterol, which alters cell morphology by extruding vesicles of cholesterol from the cell, which consequently reduces the cell surface area and rounds up the cells (Ilangumaran and Hoessli, 1998). The enzyme SMase, hydrolyses sphingomyelin into ceramide and phosphorylcholine to stimulate the internalization of cholesterol from the PM to the ER (Contreras et al., 2003; Staneva et al., 2009). Therefore, whereas MβCD entirely extrudes cholesterol from the cell, SMase internalizes the cholesterol.

Treatment of cells with MβCD resulted in the extrusion of GFP–AC8 with cholesterol in vesicles, and the small proportion of AC8 retained within the cell was expressed at the PM to increase $Ratio_{PM/Cyt}$. By contrast, SMase dramatically internalized GFP–AC8 (80%; Fig. 4A,C; supplementary material Fig. S4). It is worth noting that neither MβCD nor SMase disrupted the integrity of the actin cytoskeleton because actin filaments could still be

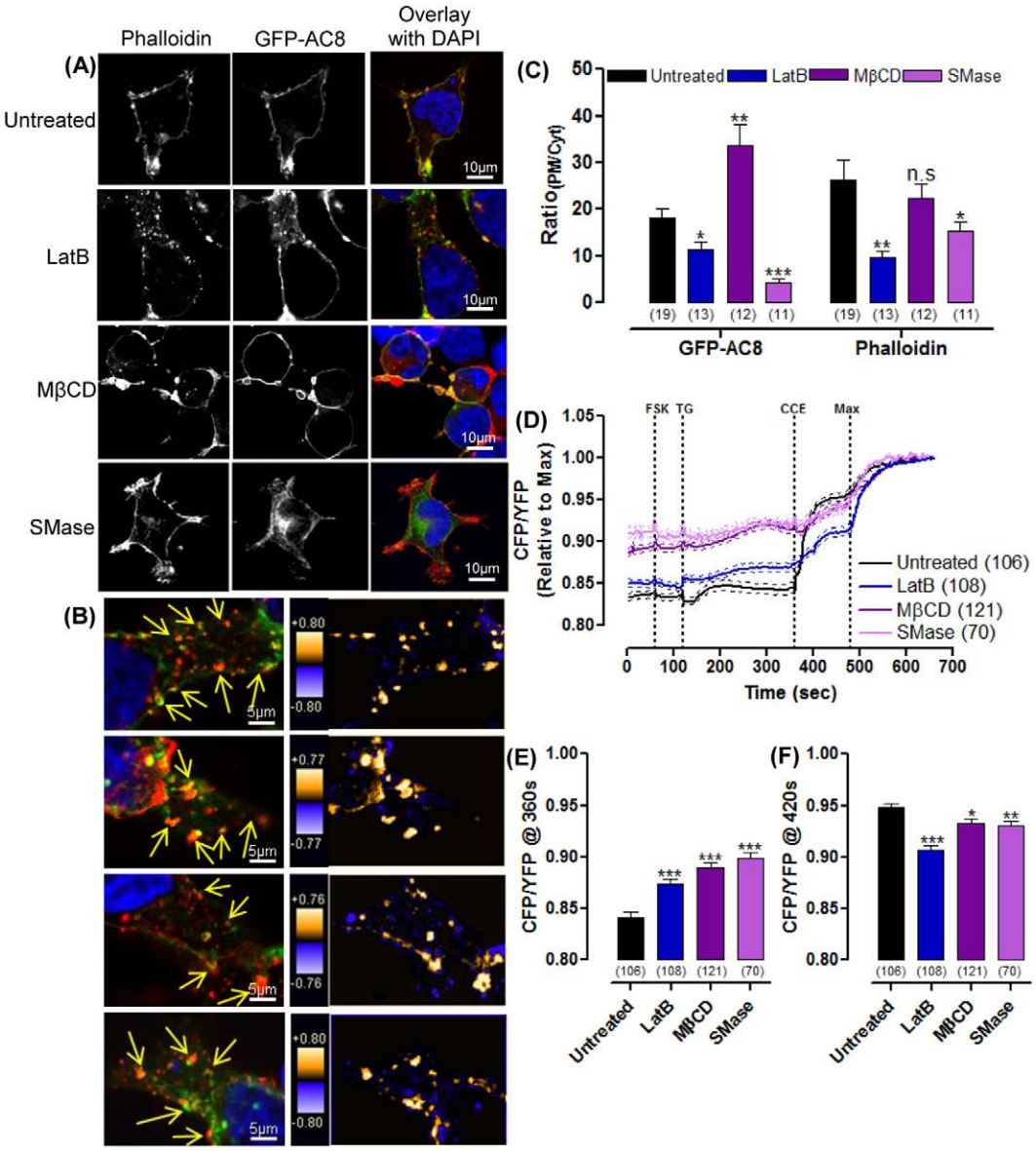

Fig. 4. GFP–AC8 distribution and regulation depends on the intact cytoskeleton and PM cholesterol. (**A**) Cells expressing GFP–AC8 pre-treated with 2 μM LatB, 10 mM MβCD or 200 mU/ml SMase, and stained with phalloidin. (**B**) Images of internalized GFP–AC8 colocalising with phalloidin (indicated by arrows) following 2 μM LatB pre-treatment; graphical representations of PDM values of colocalisation are shown in the right panels. (**C**) $Ratio_{PM/Cyt}$ analysis of A. (**D**) Single cell Epac2-camps detection of cAMP in GFP–AC8 cells pre-treated with 2 μM LatB, 10 mM MβCD or 200 mU/ml SMase, following CCE. The maximum cAMP response was induced by the addition of 10 μM FSK, 2 mM Ca^{2+}, 100 μM IBMX and 10 μM isoproterenol. (**E**,**F**) FRET ratio following TG treatment (E) and in response to CCE (F).

identified (Fig. 4A; supplementary material Fig. S3A and Fig. S4). MβCD did not alter the distribution of the actin cytoskeleton because the phalloidin signal remained enhanced at the PM, although some of the actin cytoskeleton was also extruded in the cholesterol–AC8 vesicles. Conversely, SMase, significantly internalized (41%) the actin cytoskeleton, along with AC8 and cholesterol (Fig. 4C). These data underline the strength of the interaction between AC8 and the cytoskeleton, even following raft disruption with MβCD or SMase.

Disrupting membrane rafts dramatically altered the distribution of AC8. In order to ascertain whether this redistribution affects the regulation of AC8, single-cell cAMP determinations were performed as above. As previously reported (Pagano et al., 2009), MβCD and SMase (like LatB) consistently and dramatically increased the basal accumulation of cAMP by AC8–HA (Fig. 4E), and the response to CCE was significantly reduced (Fig. 4F). To eliminate the possibility that MβCD or SMase altered AC8 activity because of a compromised Ca^{2+} response, $[Ca^{2+}]_i$ transitions were measured using Fura-2 (supplementary material Fig. S3). Following treatment with MβCD or SMase, the thapsigargin (TG)-triggered $[Ca^{2+}]_i$ rise differed somewhat although the subsequent CCE response (which regulates AC8) was unaltered.

The N-terminus of AC8 interacts with actin and cholesterol

The experiments above demonstrate that the N-terminus of AC8 interacts with actin, and this interaction controls the distribution

and regulation of AC8 (Fig. 2G, Fig. 4). In support of this conclusion, the distribution of the actin cytoskeleton is not altered when GFP–AC8M1 (which lacks the N-terminus) is expressed (Fig. 5A). Consequently, it was not surprising that the distribution of GFP–AC8M1 was not altered when the actin cytoskeleton was disrupted with LatB (Fig. 5A,B; supplementary material Fig. S5) or that LatB did not alter the regulation of GFP–AC8M1 under basal conditions or following CCE (Fig. 5C,D). These data reinforce the association between the N-terminus of AC8 and actin.

Membrane cholesterol is essential for the distribution and regulation of GFP–AC8M1

In order to determine whether the association of AC8 with the actin cytoskeleton is essential for the residence of AC8 in membrane rafts, cholesterol was depleted from cells expressing GFP–AC8M1 (which does not associate with actin) with MβCD or SMase. Similar to GFP–AC8, GFP–AC8M1 was extruded in vesicles, along with cholesterol, when cells were treated with MβCD and was internalized by SMase (Fig. 5A,B; supplementary material Fig. S5). The relative distribution of the actin cytoskeleton was not altered by MβCD or SMase treatment in these cells, reinforcing the role of the complete N-terminus in the interaction with cortical actin (Fig. 5B).

Given the dramatic effect of cholesterol depletion on the regulation of AC8, similar experiments using Epac2-camps were performed using AC8M1. Both MβCD and SMase significantly increased the basal activity of GFP–AC8M1, which precluded further stimulation by CCE (Fig. 5C,D). Thus, intact membrane rafts are essential for the proper regulation of both AC8 and the truncated AC8M1.

Given the similarity in the effect of MβCD and SMase on the distribution and regulation of AC8 and AC8M1, it might be concluded that the hydrophobic associations that drive AC8 into membrane rafts are independent of the first 106 amino acid

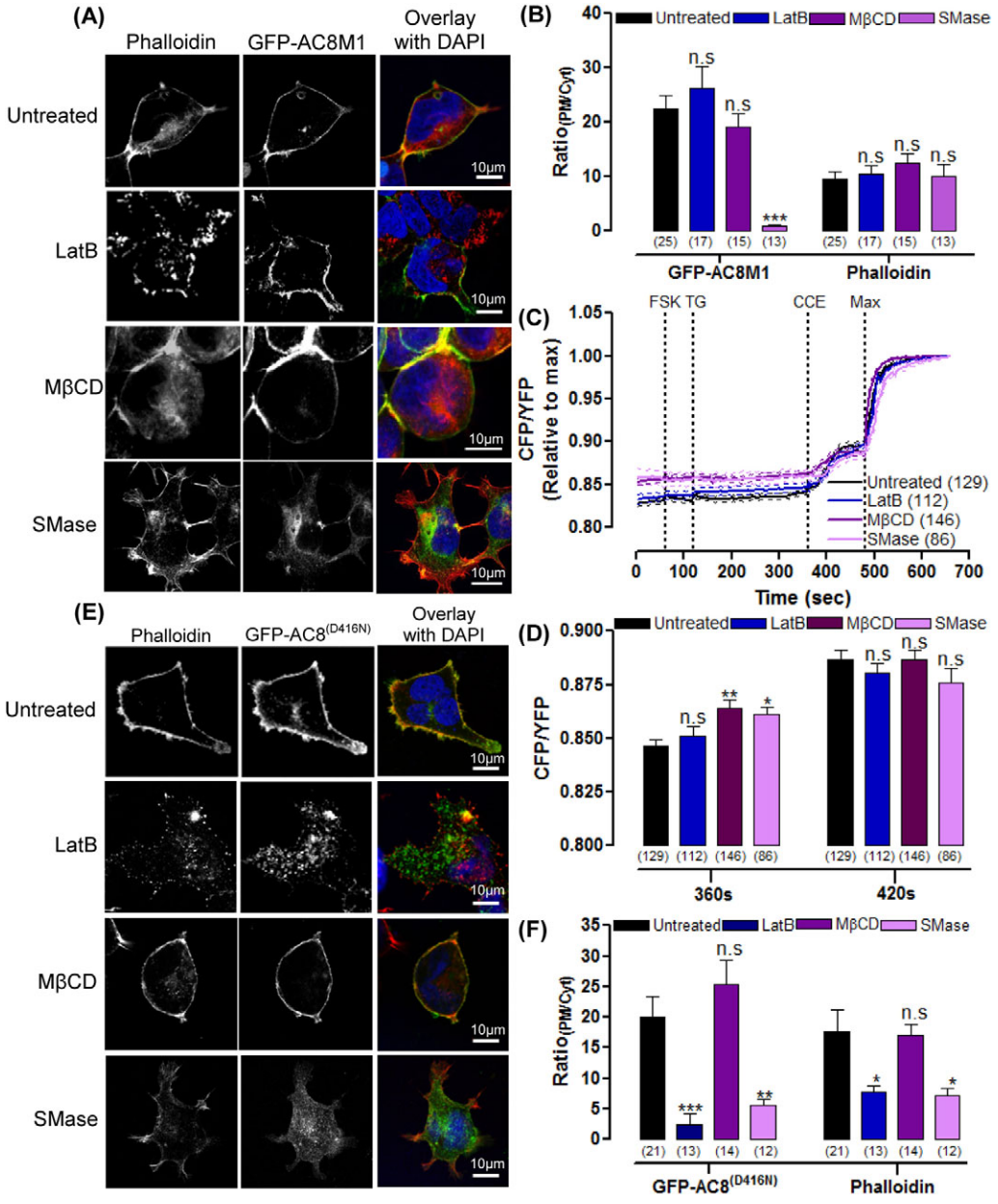

Fig. 5. The distribution and regulation of AC8 depends on its N-terminus, but not cAMP. (**A**) Cells expressing GFP–AC8M1, pre-treated with 2 μM LatB, 10 mM MβCD or 200 mU/ml SMase and stained with phalloidin. (**B**) $Ratio_{PM/Cyt}$ analysis of A. (**C**) Single cell Epac2-camps detection of cAMP in GFP–AC8M1 cells pre-treated with 2 μM LatB, 10 mM MβCD or 200 mU/ml SMase. Following CCE the maximum cAMP response was induced by addition of 10 μM FSK, 4 mM Ca^{2+}, 100 μM IBMX and 10 μM isoproterenol at 480 seconds. (**D**) FRET ratio of Epac2-camps in response to TG and CCE, from C. (**E**) Cells expressing GFP–AC8 D416N (GFP–$AC8^{(D416N)}$) pre-treated with 2 μM LatB, 10 mM MβCD or 200 mU/ml SMase and stained with phalloidin. (**F**) $Ratio_{PM/Cyt}$ analysis of E.

residues. In order to detect a direct association between AC8 and the fluorescent cholesterol surrogate, Ergosta-5,7,9(11),22-tetraen-3β-ol (ETO), acceptor bleaching FRET experiments were performed on cells expressing GFP–AC8 or GFP–AC8M1. Strikingly, the bleaching of the acceptor (GFP) led to an increase in the fluorescence emitted from the donor ETO in cells expressing GFP–AC8 (Fig. 6A,C) indicating intimate communication between the pair. However, somewhat unexpectedly, GFP–AC8M1 showed no FRET with ETO (Fig. 6B,D). Thus GFP–AC8 associates with ETO, but GFP–AC8M1 does not (Fig. 6E). However, because the previous confocal analysis (Fig. 4A, Fig. 5A) showed that membrane cholesterol contributes substantially to the distribution and regulation of both AC8 and AC8M1, it is probable that additional mechanisms consolidate the associations of AC8 in membrane rafts rather than simply an affinity for sterols.

cAMP production is essential in the AC8 association with actin, but not cholesterol

Because the full-length, but inactive, mutant GFP–AC8 D416N also enhanced cortical actin (Fig. 2G), we explored possible contributions of local cAMP production on the maintenance of the AC8–actin interaction. Following LatB treatment, GFP–AC8 D416N was significantly internalized (88%; Fig. 5E,D; supplementary material Fig. S6). Indeed, GFP–AC8 D416N was significantly more sensitive to cytoskeletal disruption than was GFP–AC8 (37% internalization), which suggests that cAMP plays, at least, a partial role in maintaining AC8 at the PM, perhaps through the known actions of PKA and/or EPAC on the polymerization of the actin cytoskeleton (Nadella et al., 2009). Thus the robust interaction between actin and AC8 that occurs through the N-terminus is reinforced by the local production of cAMP.

In order to explore the contribution of cAMP production to the residence of AC8 in membrane rafts, cholesterol was depleted from the PM using MβCD or SMase. Similar to GFP–AC8 and GFP–AC8M1, MβCD-mediated chelation of cholesterol led to the extrusion of GFP–AC8 D416N in cholesterol-containing vesicles, and SMase internalized GFP–AC8 D416N (Fig. 5E,D; supplementary material Fig. S6). Thus no obvious role was played by cAMP in the association of AC8 with lipid rafts.

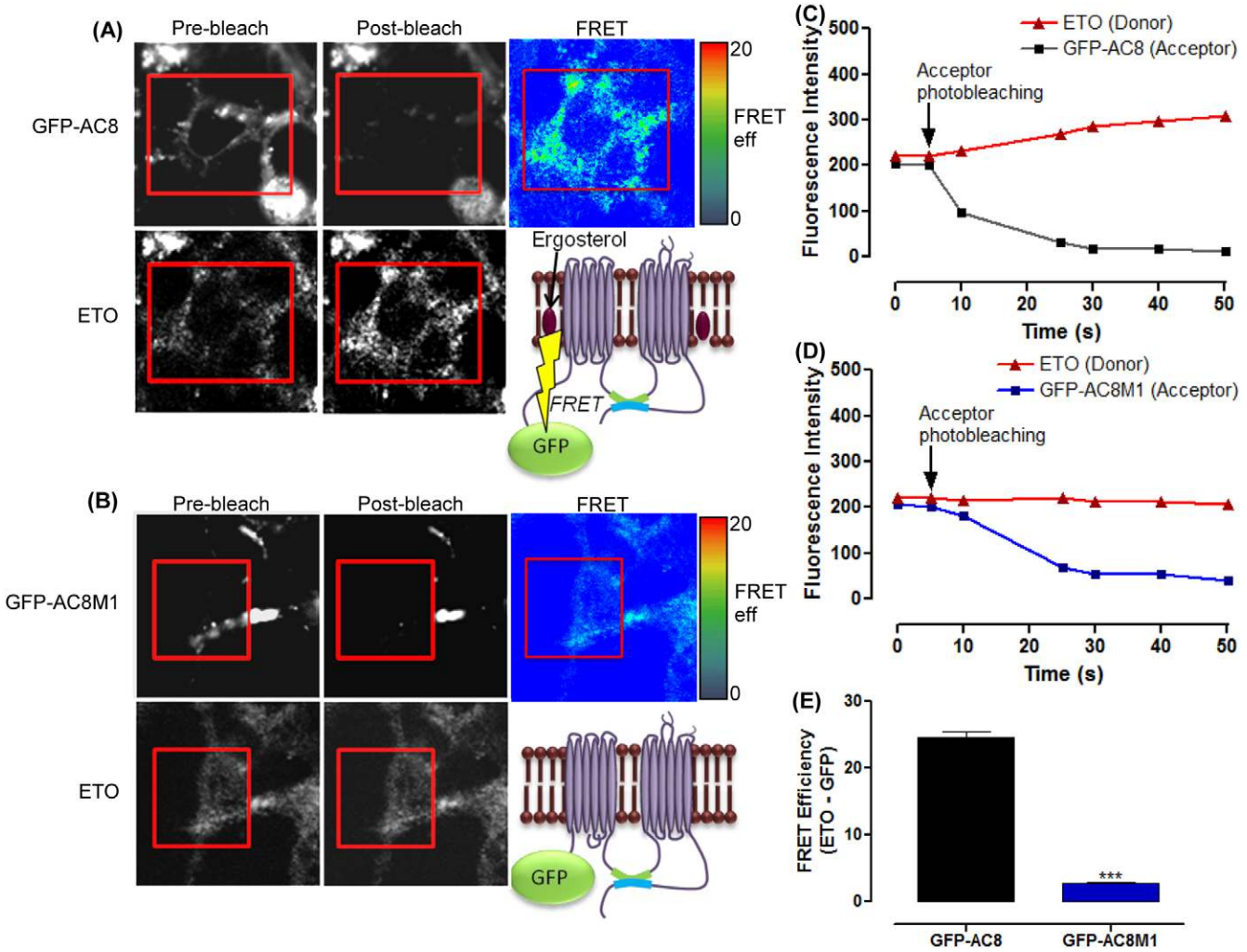

Fig. 6. Ergosterol interacts with the N-terminus of AC8. Pre-bleach, post-bleach and FRET images for ETO and (**A**) GFP–AC8 and (**B**) GFP–AC8M1. Only the areas inside the red rectangle were subject to photobleaching. (**C**,**D**) Fluorescence intensity of ETO following bleaching of (C) GFP–AC8 and (D) GFP–AC8M1. (**E**) FRET efficiency between ETO and GFP–AC8 (n=28) and GFP–AC8M1 (n=32). Data are means ± standard deviation of at least five independent transfections with the AC constructs.

The mobility of AC8 is influenced by its N-terminus

Clearly, the distribution and function of AC8 is tightly regulated by an association with actin as well as cholesterol. We felt that FRAP and fluorescence correlation spectroscopy (FCS) analysis would discern the quantitative underpinnings of this cellular association. Spot-bleach FRAP was used to quantify the diffusion coefficient (D_{FRAP}) and mobile fraction (*MF*) of GFP–AC8, GFP–AC8M1 or GFP–AC8 D416N by measuring GFP recovery into bleached regions of interest (ROI, 1.54 μm; Fig. 7A,B) and *MF* from data collected up to 200 seconds post-bleach (Fig. 7C). D_{FRAP} was calculated by recording the mean fluorescence intensity along the bleached membrane (Fig. 7D) to provide Gaussian recovery curves (Fig. 7E). When the radius of the Gaussian curves are squared and plotted against time, the slope of the subsequent straight-line graph is proportional to D_{FRAP} (5–20 seconds post-bleach, where $R^2>0.9$; Fig. 7F). To validate the data collection and analysis methods, Lyn–GFP was used as a control; the D_{FRAP} value measured was 0.81 ± 0.08 μm/second^2, which agrees with the previously published value of 0.79 ± 0.06 μm/second^2, from HEK293 cells (Hammond et al., 2009). Given the proposed interaction between the N-terminus of AC8 and the actin cytoskeleton, we anticipated that AC8M1 might move more freely in the membrane. Indeed, FRAP data confirmed that the mobility of GFP–AC8M1 differed significantly from its full-length counterparts, however, a larger proportion of GFP–AC8M1 was in fact immobile, but the mobile population diffused more quickly than GFP–AC8. Interestingly, the mobility profiles of GFP–AC8 and GFP–AC8 D416N were indistinguishable (Fig. 7C,G) suggesting that the local production of cAMP does not have any substantial influence on the mobility of AC8 in the intact cell. These data reiterate the importance of the N-terminus in constraining AC8.

FCS is an additional useful method to assess molecular diffusion in a very small confocal volume (~0.1 μm^2) by recording fluorescence fluctuations. Autocorrelation analyses of time-dependent fluctuations indicates the dwell time within the measurement volume, and subsequently, the diffusion coefficient, D_{FCS} and the number of fluorescent particles (*N*; and ultimately concentration, *N*/μm^2). Alternatively, the photon counting histogram (PCH) method analyses the amplitude of the same fluctuations and, in addition to particle number, gives a value for molecular brightness (ε), indicating the number of photons per second emitted by each molecule and therefore the extent of molecular aggregation or oligomerization. Thus, whereas FRAP accurately measures the mobility of a population of molecules within 1.54 μm^2 of a juxtanuclear region of the PM, FCS measures the diffusion of tens of molecules in real time, within a smaller area of the apical membrane (~0.1 μm^2) (Edidin, 1992; Kusumi et al., 2005). Furthermore, FCS distinguishes fast moving molecules within a microdomain, whereas FRAP detects long-range diffusion between several microdomains in the PM (Hancock and Parton, 2005; Haustein and Schwille, 2004; Lingwood et al., 2008; Pucadyil et al., 2007). However, unlike FRAP, FCS cannot reliably resolve very slow moving or immobile proteins and hence cannot determine the mobile fraction.

FCS produced comparable *D* values to those obtained with FRAP analysis and in addition determined that GFP–AC8M1 diffused more rapidly than GFP–AC8 and GFP–AC8 D416N (Fig. 7G,H). The modest variation in *D* reflects differences in the measurement area and the temperature at which the experiments were performed. All three constructs yielded a similar particle number (Fig. 7I), but PCH analysis showed that the molecular brightness of GFP–AC8M1 was significantly higher than that of either GFP–AC8 or GFP–AC8 D416N (Fig. 7J), suggesting that GFP–AC8M1 is either present in a higher multimeric form or confined within a microdomain containing more than one molecule of AC8M1.

AC8 mobility depends on membrane cholesterol

In accordance with several other studies on GFP-tagged raft proteins, such as the class II MHC (Nishimura et al., 2006), the removal of membrane cholesterol with MβCD reduced the *MF* and D_{FRAP} of GFP–AC8, GFP–AC8M1 and GFP–AC8 D416N (Fig. 8A–C) (Nishimura et al., 2006). However, a reduction in mobility of non-raft proteins following treatment with MβCD has also been observed (Kenworthy et al., 2004; Shvartsman et al., 2006; Zidovetzki and Levitan, 2007). These authors have drawn attention to additional effects mediated by MβCD that can include cytoskeletal disruption, depletion of cholesterol from non-raft regions of the PM and effects on other phospholipids. Thus caution is warranted in placing the simplest possible interpretation on the mode of action of MβCD. Treatment with SMase, like MβCD, also significantly decreased the *MF* and D_{FRAP} of GFP–AC8 (Fig. 8A–C), which reinforces the conclusion that these constructs reside in regions of the PM rich in cholesterol. However, SMase induces the formation of large aggregates of GFP–AC8 at the PM, rendering further analysis impractical (Fig. 8A).

Following treatment with MβCD, FCS, like FRAP, revealed a reduced mobility of GFP–AC8, GFP–AC8M1 and GFP–AC8 D416N (Fig. 8D). Furthermore, treatment with MβCD decreased the molecular brightness of all three constructs (Fig. 8E), whereas the particle number remained unchanged (Fig. 8F). These data support the observation from confocal imaging that all three constructs are extruded from the cell by MβCD, leaving pockets of AC8 molecules with restricted diffusion at the PM because of the absence of movement as promoted by cholesterol on lipid ordering (Nishimura et al., 2006).

AC8 mobility depends on the intact cytoskeleton

In general, if the mobility of a raft protein is curtailed by the actin cytoskeleton, then disrupting it would increase the *MF* and D_{FRAP} because of the protein is released from the constraints of the cytoskeletal corrals. This effect was seen for Na^+/K^+-ATPase (Paller, 1994). However, FRAP studies showed a decrease in the *MF* and D_{FRAP} of GFP–AC8 following disruption of the actin cytoskeleton with LatB (Fig. 8B,C), suggesting that AC8 is not simply released from corrals. Rather, the AC8-actin association persists, forming large aggregates of GFP–AC8 and actin as seen at the PM in confocal studies. These aggregates reduce the D_{FRAP} and thus prevent inhibitory and stimulatory constraints from interacting with AC8, precluding normal regulation. In contrast to FRAP analysis, treatment with LatB significantly increased the D_{FCS} of GFP–AC8 (Fig. 8D). However, the molecular brightness and particle number were not altered by LatB, indicating that the aggregation or oligomerization state of GFP–AC8 did not change (Fig. 8E,F). Therefore the GFP–AC8 aggregates detected at the PM in confocal studies are slow moving and so become bleached. Only non-aggregated material is measured by FCS, resulting in an overall increase in the diffusion of AC8.

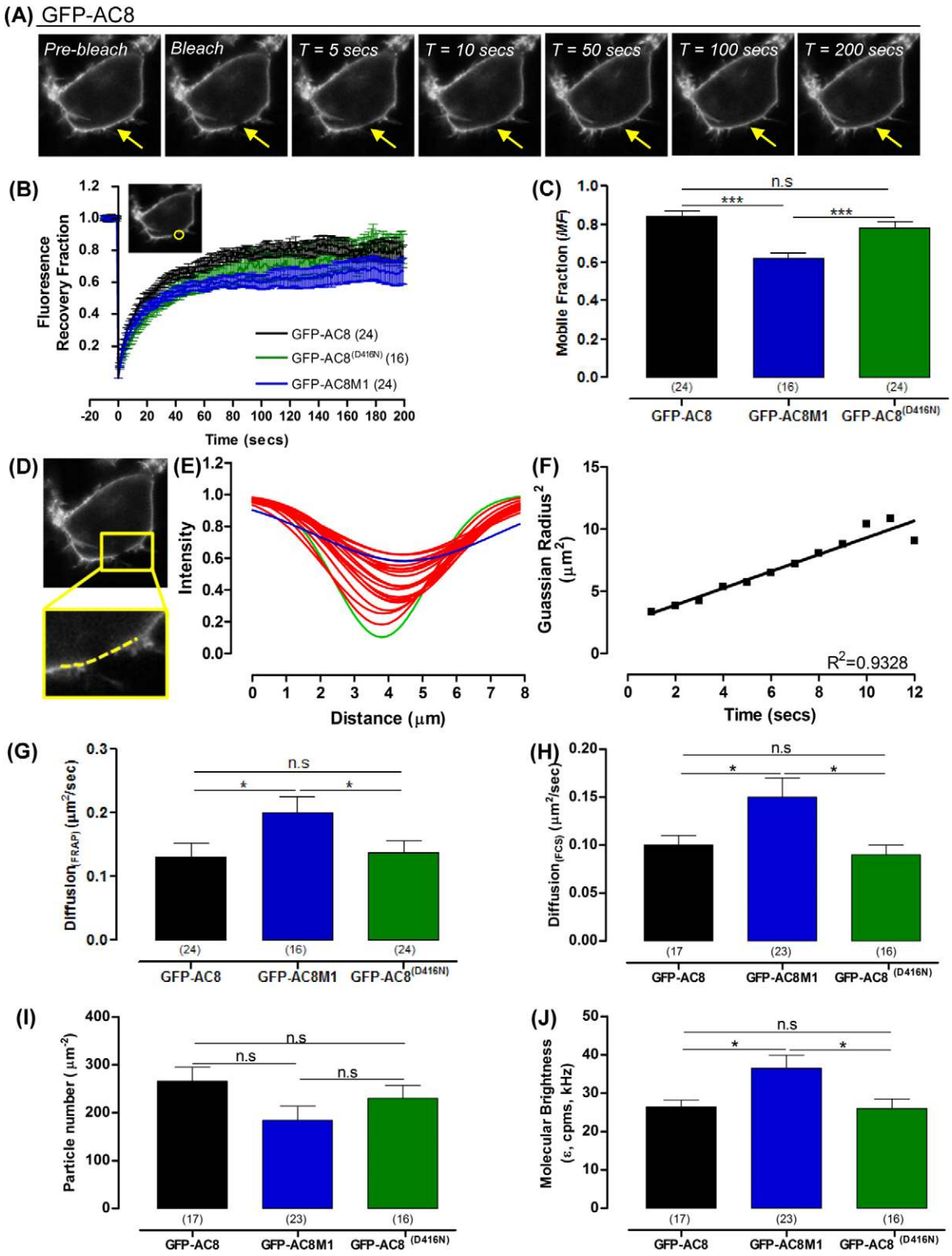

Fig. 7. The N-terminus of AC8 defines its mobility. (**A**) Time-lapse series of a live cell expressing GFP–AC8. (**B**) Recovery curves of GFP–AC8, GFP–AC8M1 and GFP–AC8 D416N (GFP–AC8$^{(D416N)}$) fluorescence intensities within the bleached membrane ROI (1.86 μm^2). (**C**) *MF* of GFP–AC8, GFP–AC8M1 and GFP–AC8 D416N as determined by the Y_{MAX} of the recovery curves. (**D**) Image of GFP–AC8 cell 1 second post-bleach with the linear ROI (dashed line) across the bleached membrane to record intensities. (**E**) Representative Gaussian profiles from D for 20 seconds post-bleach (green, 1 second; blue, 20 seconds; red, 2–19 seconds post-bleach). (**F**) Example of the radius squared from E, where the goodness of fit (R^2) is greater than 0.9. (**G**) D_{FRAP} as determined by the slope of F. (**H**) D_{FCS} of GFP–AC8, GFP–AC8M1 and GFP–AC8 D416N. (**I**) Particle number (μm^{-2}) of GFP–AC8, GFP–AC8M1 and GFP–AC8 D416N. (**J**) Molecular brightness (ε, cpms, kHz) of GFP–AC8, GFP–AC8M1 and GFP–AC8 D416N.

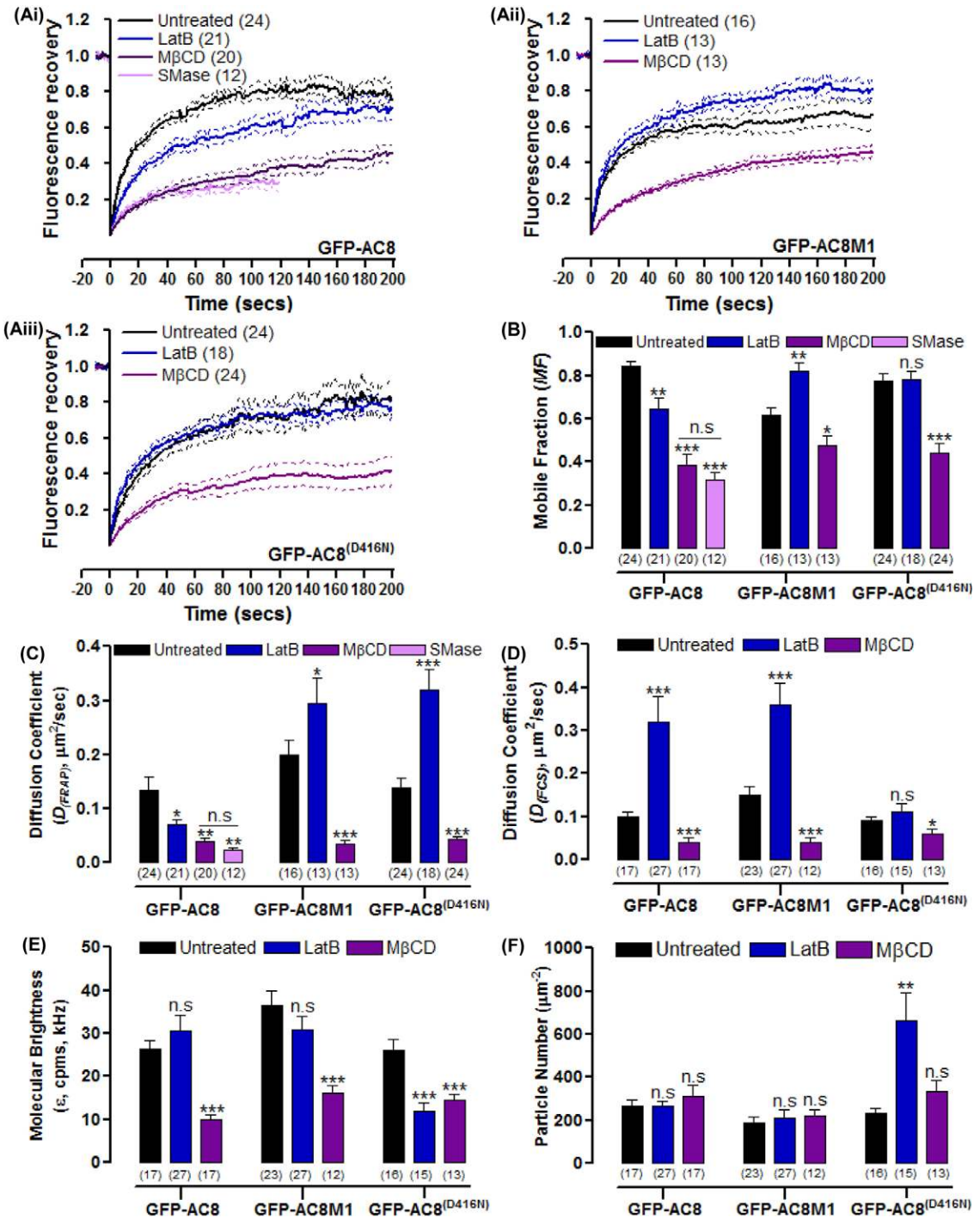

Fig. 8. Both the N-terminus of AC8 and cAMP production influences AC8 mobility. (**A**) Recovery curves of cells expressing GFP–AC8, GFP–AC8M1 or GFP–AC8 D416N (GFP–AC8$^{(D416N)}$) and pre-treated with 2 μM LatB, 10 mM MβCD or 200 mU/ml SMase. (**B**) *MF* from A. (**C**) D_{FRAP} from A of GFP–AC8, GFP–AC8M1 or GFP–AC8 D416N pre-treated with 2 μM LatB or 10 mM MβCD. (**D**) D_{FCS} of GFP–AC8, GFP–AC8M1 or GFP–AC8 D416N pre-treated with 2 μM LatB or 10 mM MβCD. (**E**) Molecular brightness (ε, cpms, kHz) of GFP–AC8, GFP–AC8M1 and GFP–AC8 D416N. (**F**) Particle number (μm^{-2}) of GFP–AC8, GFP–AC8M1 and GFP–AC8 D416N.

Because AC8 enhances the cortical actin, but the N-terminally truncated mutant AC8M1 does not, the effect of LatB treatment on the mobility of AC8M1 was investigated. In contrast to GFP–AC8, LatB treatment increased the *MF* and D_{FRAP} of GFP–AC8M1 (Fig. 8B,C). Interestingly, consistent with the FRAP data, D_{FCS} of GFP–AC8M1 also increases following LatB treatment and the brightness and particle numbers are unaltered (Fig. 8D–F). Collectively, these data are consistent with the idea that GFP–AC8M1 is transiently trapped within actin cytoskeleton corrals and is simply released upon cytoskeletal disruption with

LatB (Fig. 9). Thus, we propose that the N-terminus of AC8 associates with the actin cytoskeleton, enhancing cortical actin by consequently recruiting the filamentous meshwork to the PM, which restricts the diffusion of AC8 to tracking the path of the filaments that lie beneath the PM (Fig. 9B). However, without the N-terminus, in a similar manner to Kv2.1 channels (O'Connell et al., 2006; Tamkun et al., 2007), AC8M1 is transiently trapped within actin cytoskeleton corrals, constrained by the perimeters created by the actin meshwork (Fig. 9B). The large cytosolic domain of AC8M1 (C1 and C2 regions of approximately 72 kDa), could be sterically hindered by the cytoskeleton. Such restrictions are also seen in the transport protein, band 3, where cleavage of the cytosolic domain (approximately 40 kDa) allows the protein to move freely (Tomishige et al., 1998). However, at this stage, the model presented (Fig. 9) is speculative and not detailed; in particular, the corrals and membrane domains might, in part, be established through the spectrin membrane skeleton. The relationship between the membrane skeleton and cortical actin rim should be experimentally addressed in future studies as should the impact of disruptors such as LatB on the discrete pools of actin, which might have differing effects on the gelation state of the cytoskeleton at the PM.

The contribution of cAMP to the AC microdomain

The production of cAMP by ACs offers an increased opportunity for ACs to sculpt their microdomain. Careful observation revealed colocalisation 'hot spots' between AC8 and phalloidin (Fig. 1B, Fig. 2E, Fig. 4A), which was far more prevalent than in cells expressing AC8 D416N (Fig. 2E, Fig. 5E). Given that confocal image analysis indicated that local cAMP contributes to the maintenance of AC8 at the PM from the increased sensitivity of the catalytically inert AC8 mutant to cytoskeletal disruption (Fig. 4B, Fig. 5E), the mobility of GFP–AC8 D416N following treatment with LatB was investigated. Treatment with LatB dramatically increased the D_{FRAP} of GFP–AC8 D416N, whereas the *MF* was not altered. These data indicate that cAMP production selectively influences AC8 mobility (Fig. 8B,C).

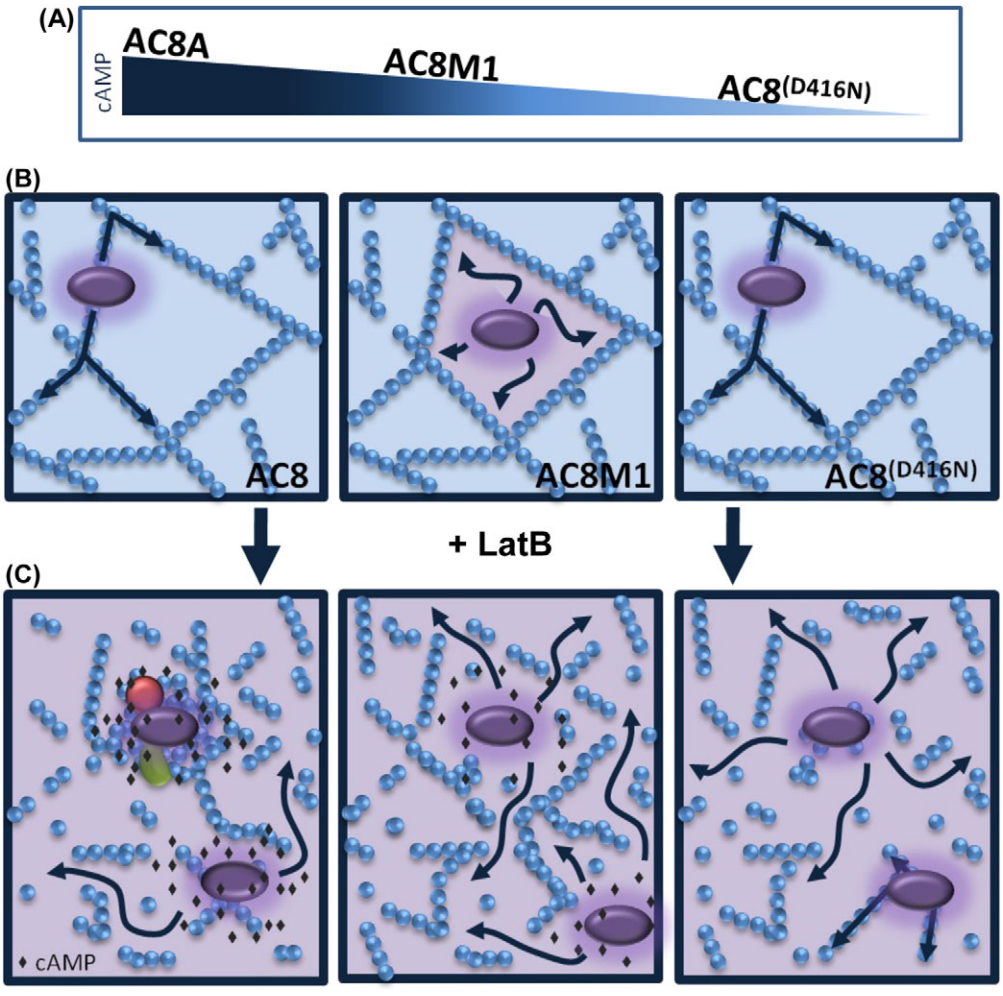

(D)

		GFP-AC8	GFP-AC8M1	GFP-AC8(D416N)
FRAP	MF	- -	+ +	n.s
	$D_{(FRAP)}$	-	+	+ + +
FCS	$D_{(FCS)}$	+ + +	+ + +	n.s

Fig. 9. Representation of the actin cytoskeleton in the AC8 microdomain. (**A**) Depiction of the relative activities of AC8, partially active AC8M1 and inactive AC8 D416N (GFP–AC8$^{(D416N)}$). (**B**) AC8, AC8M1 and AC8 D416N microdomains with respect to the cytoskeleton. In the intact cell, AC8 and AC8 D416N are tethered by the N-terminus to F-actin (blue spheres). AC8M1 lacks the N-terminus and is trapped in corrals. (**C**) Following disruption with LatB, the cAMP (black diamonds) produced by AC8 could promote protein–protein interactions (green and red shapes) and induce actin polymerization, forming slow moving aggregates, which can be measured by FRAP and bleached by FCS, and a fast moving, non-aggregated population. Disruption of the cytoskeleton leads to the free diffusion of AC8M1 and two populations of AC8 D416N are produced, both recordable by FRAP and FCS; fast diffusing individual proteins and slower moving proteins bound to small linear actin filaments. (**D**) Summary of FRAP and FCS data following treatment with LatB. Addition and subtraction signs represent an increase or decrease, respectively, compared with the untreated control.

Interestingly, the D_{FCS} of GFP–AC8 D416N was not altered with LatB (Fig. 8D). However, there was a significant reduction in molecular brightness (Fig. 8E), with a corresponding increase in particle number (Fig. 8F). The FCS and FRAP data, when considered together, confirm the observation that aggregates of GFP–AC8 D416N were dramatically internalized (88.2%) following treatment with LatB, leaving only monomeric proteins at the membrane. These monomers are likely to be present in two populations: individual proteins that diffuse quickly, and slower moving proteins bound to small linear actin filaments or aggregates. Because FRAP records the diffusion of AC8 D416N over larger distances, it is unlikely to detect the cytoskeletal hindrance distinguishable by FCS (Fig. 8C). The discrepancy between the effects of LatB on GFP–AC8 and GFP–AC8 D416N therefore reflects the basal cAMP produced by GFP–AC8 within its microdomain. There is a large body of literature that describes the effect of cAMP, through the actions of PKA and EPAC, on the structure, remodelling and polymerization of the actin cytoskeleton (Howe, 2004; Nadella et al., 2009). Our data are in agreement with these findings and illustrate that even following cytoskeleton disruption, local cAMP produced by AC8 could induce the polymerization of actin, perhaps through the LIM kinase-1 pathway (Nadella et al., 2009), forming actin aggregates around AC8, thus trapping it and reducing its mobility.

PKA inhibition alters AC8 mobility following actin disruption

Because the cAMP target, PKA, has a major function in the structure and integrity of the actin cytoskeleton, we wondered whether the mobility of AC8 would resemble that of AC8 D416N following PKA inhibition. PKA inhibition by H89 or KT5720 did not significantly alter the *MF* and D_{FRAP} of GFP–AC8 in the intact cell (Fig. 10A). However, PKA inhibition prevented the decrease in the *MF* of GFP–AC8 following cytoskeleton disruption (Fig. 10A) and significantly increased D_{FRAP}, compared with control cells treated with LatB (Fig. 10B). Therefore, the mobility of GFP–AC8 in the presence of the PKA inhibitors resembles that of GFP–AC8 D416N when cells were treated with LatB. Consequently AC8 by producing cAMP, and thereby (through PKA) remodelling the actin cytoskeleton, influences its mobility by altering the cytoskeletal framework of its microdomain.

The expression of AC8 and cAMP analogues partially ‘rescue’ GFP–AC8 D416N mobility

To pursue further the role of cAMP in modulating the AC8 microdomain, we asked whether exogenous cAMP analogues or the co-expression of untagged (but live) AC8 would ‘rescue’ the mobility of inactive GFP–AC8 D416N. Because cAMP activates both PKA and EPAC, but there are no available inhibitors of Epac, two cAMP analogues were used: chlorophenylthio–cAMP (CPT–cAMP), which specifically activates EPAC, and dibutyryl–cAMP (DB–cAMP), which is a potent PKA activator (Enserink et al., 2002). CPT–cAMP significantly decreased the mobility of GFP–AC8 D416N when the actin cytoskeleton was disrupted with LatB (Fig. 10C,D) and DB–cAMP reversed the effect of LatB on the D_{FRAP} of GFP–AC8 D416N so that disrupting the cytoskeleton no longer significantly increased the diffusion (Fig. 10D). These data suggest that these cAMP analogues can indeed alter the GFP–AC8 D416N microdomain, partially converting the dynamic behaviour of GFP–AC8 D416N to be similar to that of GFP–AC8, when the actin cytoskeleton is disrupted. A similar effect was recorded in cells coexpressing AC8–HA and GFP–AC8 D416N; the local cAMP produced by AC8 partially ‘rescued’ the mobility of AC8 D416N when cells were treated with Lat B (Fig. 10E,F). These experiments support a role for local cAMP in shaping the architecture of the AC8 microdomain.

AC8 interacts with the plus end of the actin filament

In order to define the nature of the AC8–actin association, actin perturbants other than LatB were used. Cytochalasin D (CytD) directly binds to and terminates the plus end of the actin fibres to prevent polymerization of actin filaments, inducing them to contract, whereas jasplakinolide (Jasp) binds the length of the actin filament and induces polymerization of G-actin onto growing filaments leading to the overall disruption of F-actin. (Note, however, that Jasp competes with phalloidin for actin, precluding the monitoring of actin disruption using phalloidin.)

To compare the effects of CytD and Jasp, with that of LatB, on the distribution, regulation and mobility of GFP–AC8, GFP–AC8M1 and GFP–AC8 D416N, cells were incubated with 30 μM CytD or 1 μM Jasp and analyzed as before. Somewhat unexpectedly, neither CytD nor Jasp altered the distribution of GFP–AC8, GFP–AC8M1 or GFP–AC8 D416N (supplementary material Fig. S7A–C). Relative distribution analysis confirmed that all three constructs remained at the PM and were not internalised (supplementary material Fig. S7D). Because LatB compromised the regulation of GFP–AC8 by CCE, cAMP accumulation assays were performed on cell populations expressing GFP–AC8 or GFP–AC8M1 following treatment with CytD or Jasp. Interestingly, neither treatment altered the activity of GFP–AC8 or GFP–AC8M1 (supplementary material Fig. S7E). Furthermore, FRAP analysis revealed that CytD and Jasp did not alter the mobility of GFP–AC8, GFP–AC8M1 or GFP–AC8 D416N (supplementary material Fig. S7F,G).

Because neither CytD nor Jasp altered AC8 mobility, association with the cytoskeleton is unlikely to impede the diffusion of AC8 at the PM. It is not uncommon for different cytoskeletal disruptors to have differing consequences; for example, Lat B, but not CytD, increased the diffusion of MHC-II (Umemura et al., 2008). The intriguing differences in the effects of each actin cytoskeleton disruptor must be attributed to their varying mechanisms of action. CytD and Jasp associate with the plus end of the actin filament, so it is probable that AC8 interacts with this region of the filament and is perhaps displaced by CytD and Jasp. However, LatB binds to G-actin and passively degrades the actin filaments around AC8, permitting the accumulation of short filaments around AC8, as seen in confocal images (Fig. 4B), and prevents access to the catalytic site, impeding regulation by CCE (Fig. 4F).

Discussion

This study has substantially expanded our conception of the AC8 microdomain. We conclude that AC8 resides in a cholesterol-rich membrane environment that is stabilized by the actin cytoskeleton. In addition, a substantial contribution of cAMP was highlighted in the structural integrity and remodelling of the actin cytoskeleton that ultimately has a major influence on the mobility and regulation of AC8 in its own microdomain.

The perception of membrane rafts has evolved considerably over the last decade, and although the term may not be entirely

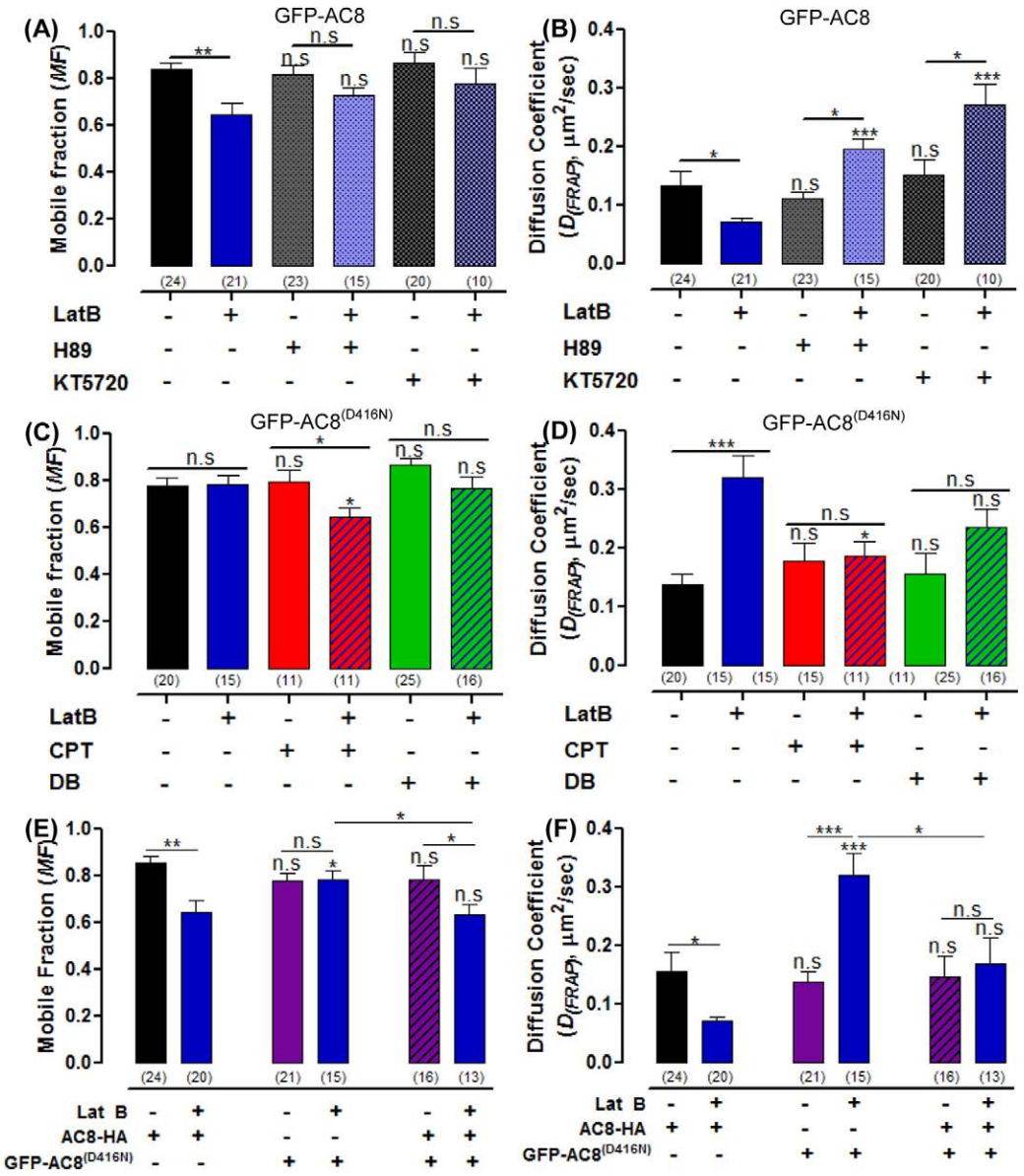

Fig. 10. cAMP influences the cytoskeleton through PKA and EPAC. (**A**,**B**) The effect of inhibiting PKA with 10 μM H89 or 1 μM KT5720 on (A) the *MF* of GFP–AC8 ± LatB and (B) D_{FRAP} of GFP–AC8 ± LatB. (**C**,**D**) The effect of exogenous cAMP analogues, CPT–cAMP and DB–cAMP on (C) the *MF* of GFP–AC8 D416N ± LatB and (D) the D_{FRAP} of GFP–AC8 D416N ± LatB. (**E**,**F**) The effect of LatB on the mobility of GFP–AC8 D416N when AC8–HA is also expressed on (E) the *MF* and (F) the D_{FRAP}.

apt because these regions are not likely to have definitive perimeters, but rather gradients of cholesterol and sphingolipids, the residence of AC8 in rafts and close association with cholesterol is essential for its regulation and mobility. The association of AC8 with cholesterol could support the formation of the AC8 microdomain by accumulating hydrophobic regulatory proteins, scaffold proteins and effectors to permit stringently controlled cAMP signal propagation.

An association between the actin cytoskeleton and a transmembrane raft protein, such as AC8, is not atypical; several such interactions have been described and are essential for membrane protein regulation, signal propagation and cell structure (Chichili and Rodgers, 2007; Langhorst et al., 2007; Stahlhut and van Deurs, 2000). The binding of actin to AC8 in the resting cell might have significance as an allosteric modulator, altering the binding affinities of other associated proteins. For instance, upon the induction of CCE, the binding of actin can be displaced by Ca^{2+}–CaM to allow the activation of AC8, so that the spatiotemporal dependence of the N-terminal associations could be affected not only by cAMP but also by Ca^{2+}. The behaviour of AC8 following cytoskeletal disruption resembles that of other membrane proteins, including Na^{+}/H^{+} exchanger type 3 (NHE3) (Cha et al., 2004) and $Ca_v1.3$ voltage-gated Ca^{2+} channels (Cristofanilli et al., 2007), which are internalized following treatment with LatB. However, the intricacy of the relationship with the actin cytoskeleton, resulting from the effect of cAMP, is unique to AC8. The nature of the complex involved requires further investigation, and

might be cell-type specific, but it potentially involves AKAP79, which binds both AC8 and actin (Willoughby et al., 2010b; Dell'Acqua et al., 2006). Alternatively, actin also binds to ezrin, which interacts with Na^+/H^+ exchanger regulatory factor 1 and 2, which in turn, binds to NHE3 (Cha et al., 2004). The NHE3 variant, NHE1 is considered to be an essential component of the AC8 microdomain, protecting the enzyme from cellular pH swings (Willoughby et al., 2005).

The indication that AC8 associates with the plus end of the actin filament suggests that small linear actin filaments remain attached to AC8 following disruption with LatB, effectively and dramatically immobilising AC8 within the membrane. Interestingly, the mobility of NHE3 and cystic fibrosis transmembrane conductance regulator (CFTR) were also decreased following treatment with LatB, as determined by FRAP analysis. Both of these proteins interact with the actin cytoskeleton (Cha et al., 2004; Haggie et al., 2004). In fact, NHE3 not only interacts with the actin cytoskeleton, but also with CaM and PP2A, both of which bind the N-terminus of AC8 (Crossthwaite et al., 2006; Gu and Cooper, 1999). Furthermore, NHE3 mobility is inhibited by cAMP (Cha et al., 2004) and following LatB treatment it also becomes internalized and has a decreased *MF* at the PM (Cha et al., 2004). Thus, AC8 and NHE3 are very similar in their dynamic behaviour and it is interesting to note the application of similar cellular strategies in managing these proteins.

We believe there is interdependence between the association of AC8 with cholesterol rafts and the actin cytoskeleton; however, we cannot tell whether there is a primacy in the two associations. It is conceivable that as a consequence of the apparently tight association of AC8 with the actin cytoskeleton, and the direct binding of cholesterol, that AC8 orchestrates its own microdomain, possibly recruiting other raft-associated proteins or elements of the CCE apparatus (Pani et al., 2008). This gives rise to the essential residence of AC8 in raft domains for its regulation by CCE.

How AC8 is targeted to raft domains or binds to cholesterol is unknown. Recent investigations have revealed sequence motifs involved in directing proteins into raft nanodomains, including lysine-rich regions that occur in a cytoplasmic, membrane-proximal location (Rossin et al., 2010), cholesterol recognition and/or interaction amino acid consensus (CRAC) sequences (Li and Papadopoulos, 1998) and a stretch of positively charged amino acid residues (Popik and Alce, 2004). In fact, AC8 contains five CRAC motifs, and 28% of the 50 amino acids preceding the first transmembrane domains are positively charged. Whether these regions play a role in AC8 targeting remains to be determined.

The strength of the AC8–actin interaction suggests that this property is exploited and regulated. Importantly, within the present context, the transience of the actin cytoskeleton is driven by its state of polymerization, which is regulated by several factors including Ca^{2+} and cAMP (dos Remedios et al., 2003; Maciver and Hussey, 2002; Ruppelt et al., 2007). Thus it would not be surprising if cAMP reinforced the AC8–actin association whereas Ca^{2+} prevented the interaction. By such means one could have a staggered loosening and tightening of the association, which could play a crucial role in the migration of AC-led processes within the PM. The significance of this association in an intact cell might become apparent in the context of cellular functional domains, such as in focal adhesion complexes, which could be influenced by local concentrations of Ca^{2+} and cAMP. It might not be too fanciful to envisage a role for the ACs as the core of a signalling hub around which essential regulatory elements are recruited, the full significance of which will only become apparent in demanding regulatory environments, such as hippocampal neurons, where this enzyme naturally resides. Hence the present study might have opened the door on AC-based functional microdomains that serve not only to protect the enzyme and optimize its regulation by upstream regulators, such as Ca^{2+}-entry, and downstream effectors, such as PKA and EPAC, but also the assembly of a mobile cohort of gross cellular organizational factors.

Materials and Methods

Reagents and constructs

The rabbit polyclonal anti-AC8 antibody was a kind gift from Jim Cali (Promega, Madison, WI, USA). Epac2-camps was a gift from Martin Lohse (Würzberg University, Germany) (Nikolaev et al., 2004).

GFP–AC8 was generated by cloning AC8 cDNA between the *Apa*I and *Xba*I restriction sites of pEGFP-C1. GFP–AC8 D416N (Tesmer et al., 1999) was introduced by site-directed mutagenesis according to the QuickChange protocol (Stratagene, La Jolla, CA) using the fusion high-fidelity polymerase kit (Finnzymes) according to manufacturer's instructions, using the forward and reverse primer sequence, 5′-CGAGAACGTCAGTATTCTTTTTGCAAATGTCAAAGGATTTA-C-3′ and 5′-GAGAGGTTGGTAAATCCTTTGACATTTGCAAAAAGAATAC-3′, respectively. Lyn–GFP, the modified N-terminus of Lyn kinase (MGCIKSKGKDS), was a gift from T. Meyer (Stanford University, Stanford, CA) and was cloned into pEGFP-N1 (Clontech Laboratories) between the *Eco*RI and *Bam*HI sites.

Cell culture and immunocytochemistry

HEK293 cells were cultured in Eagle's minimal essential medium (EMEM) supplemented with 10% (v/v) fetal bovine serum, 50 μg/ml penicillin, 50 μg/ml streptomycin and 2 mM L-glutamine, and maintained at 37℃ in a humidified atmosphere of 5% CO_2. The Lipofectamine 2000 method of transfection was used according to the manufacturer's instructions. After 48 hours, 800 μg/ml G-418 disulphate was added to select for transfected cells, which was reduced to 400 μg/ml after 48 hours.

Where appropriate, cells were incubated with 2 μM LatB, 10 mM MβCD or 200 mU/ml SMase in cell growth medium, for 1 hour at 37℃. Live cells were incubated with WGA (5 μg/ml), 3 minutes before fixing in 4% (v/v) paraformaldehyde for 10 minutes. Cells stained with phalloidin or anti-tubulin were permeabilized [0.1% (v/v) Triton X-100 for 10 minutes] and blocked [10% (v/v) goat serum for 1 hour];. Cells were incubated with phalloidin (1 IU/ml, 2 hours) or mouse anti-tubulin antibody [6 μg/ml, diluted in 1.5% (v/v) goat serum for 1 hour]. After rinsing in phosphate-buffered saline (PBS; 137 mM NaCl, 2.7 mM KCl, 10 mM Na_2HPO_4, 1.76 mM KH_2PO_4, pH 7.4), cells were incubated with Alexa-Fluor-555-conjugated goat anti-mouse antibody (10 μg/ml for 1 hour), followed by a final rinse in PBS. Non-specific binding could not be detected, nor could a significant fluorescent signal, when either the primary or the secondary antibody was added alone. All coverslips were mounted in Vectashield with DAPI.

AC in vitro activity assay

Crude membranes were prepared and AC activity was measured in vitro as described previously (Nakahashi et al., 1997; Boyajian et al., 1991).

Single cell cAMP measurements

Cells transiently expressing Epac2-camps were equilibrated at room temperature in HEPES-buffered saline (HBS; 140 mM NaCl, 4 mM KCl, 0.2 mM $MgCl_2$, 11 mM D-glucose and 10 mM HEPES, pH 7.4) containing 0.5 mM Ca^{2+}. CCE was triggered following a pretreatment with 200 nM TG in HBS in the absence of Ca^{2+} (plus 100 μM EGTA) followed by the addition of 0.5 mM or 2 mM CaCl2 for AC8 and AC8M1, respectively, and in the presence of 10 nM FSK to potentiate CCE-dependent AC activity. A saturating FRET signal was stimulated [10 μM FSK, 2 mM Ca^{2+}, 100 μM 3-isobutyl-1-methylxanthine (IBMX) and 10 μM isoproterenol] at the end of each experiment. Fluorescence was measured using an Andor CCD Ixon+ camera and Optosplit (505DC, Cairn Research, Faversham, UK) as described previously (Wachten et al., 2010) and analyzed using Metamorph software (Molecular Devices). Cells in which the CFP and YFP fluorescence intensity was less than twice the background signal were excluded, as were cells with excessive expression of the probe. Data were plotted as changes in the 470 nm/535 nm (CFP/YFP) emission ratio normalized to maximum FRET change for each cell.

Single cell Ca^{2+} measurements

Cells were loaded with 2 μM Fura-2/AM and 0.02% (v/v) Pluronic F-127 for 40 minutes with 2 μM LatB, 10 mM MβCD or 200 mU/ml SMase in cell growth medium at 37℃. Cells were incubated for a further 20 minutes in fresh pharmacological disruptor. Cells were washed in HBS with 0.5 mM Ca^{2+} before pre-treating with 200 nM TG in 0 mM Ca^{2+} HBS (100 μM EGTA), and CCE was triggered with 0.5 mM external Ca^{2+}. Maximum fluorescence (F_{Max}) was obtained with 5 μM ionomycin and 10 μM Ca^{2+} to saturate the Fura-2 signal. Ca^{2+} traces are relative to the fluorescence ratio at 0 minutes (F/F_0) and normalised to the maximum ratio change for each cell. Cells were imaged using a CoolSNAP-HQ CCD camera (Photometrics) and monochromator system (Cairn Research) and analysed using MetaFluor software (Molecular Devices) (Wachten et al., 2010).

Acceptor bleaching FRET

The FRET efficiency between GFP–AC8 or GFP–AC8M1 (donor) and Ergosta-5,7,9(11),22-tetraen-3β-ol (ETO; acceptor) a cholesterol fluorescent analogue, was monitored using an FV1000 Olympus spectral confocal microscope in combination with the acceptor bleaching FRET technique. ETO was purchased from Sigma (cat. no. E2634). The cholesterol analogue was excited at 420 nm, peak emission occurs at 488 nm, which coincides with the excitation maxima for GFP, making this cholesterol analogue an excellent FRET pair. HEK293 cells expressing GFP–AC8 or GFP–AC8M1 were incubated for 10 minutes with the cholesterol fluorescent analogue used at a final concentration of 5 μM. Images were obtained at a rate of 1 every 5 seconds for the duration of the experiments. Pre- and post-bleaching fluorescence was determined for each individual experiment in the same cells. FRET efficiency was calculated as previously described (Salgado et al., 2008). All experiments were corrected for fluorescence bleed-trough before calculating FRET efficiency.

Confocal imaging and spot-bleach FRAP

Confocal images (1 μm optical slice thickness) were captured with a Leica SP5 TCS laser scanning confocal microscope attached to a DM16000 inverted microscope, equipped with a 63× plan-apochromatic 1.4 NA oil immersion objective (Leica) running the Leica Application Suite (LAS) AF Leica software, version 1.8.2. Cellular DAPI and GFP were visualized using the 405 nm and 488 nm line of an argon ion laser, and collected at 415–455 nm and 495–545 nm, respectively. Cells stained with Alexa Fluor 555 or Alexa Fluor 568 were visualized using the 543 nm line of a HeNe laser and collected between 615 and 700 nm. Cells expressing single fluorophores were used to adjust the laser emission and collection spectra to eliminate bleed-through into different channels. Graphical representations of product of the differences from the mean (PDM) values (n) were calculated using ImageJ where PDM = (red intensity – mean red intensity) × (green intensity – mean green intensity). Pseudocolour yellow represents colocalisation, whereas pseudocolour blue is where colocalisation is absent.

Cells were plated on glass coverslip inserts coated with poly-L-lysine for 24 hours and imaged on a Leica SP5 confocal microscope, in an environmental chamber at 37℃ (Solent Scientific, Segensworth, UK). For maximum light acquisition and to defocus the bleaching light beam to effectively bleach GFP either side of the focal plane, the pinhole was fully opened to an optical section of approximately 5 μm. FRAP experiments were performed according to the FRAP wizard in the LAS AF software. Images were scanned bidirectionally at maximum speed (1400 Hz) with a single line average to reduce noise, using the 488 nm line of an argon ion laser and collected between 500 and 575 nm. Images (256×256 pixels) were acquired at a rate of 1 frame/second. Ten pre-bleach frames were acquired with a laser power of 5–8% before bleaching the membrane proteins (100 mseconds, 80% argon laser at 100% transmission) using a spot bleach protocol with the laser focused on the PM. Fluorescence recovery was followed for 200 seconds, with a laser power of approximately 5–8% to ensure full recovery.

Estimating the *MF* and D_{FRAP}

The mobile fraction (MF) and diffusion coefficient $(D)_{FRAP}$ were calculated as previously described (Hammond et al., 2009; Oancea et al., 1998). In brief, Leica (lif) image stacks from FRAP spot bleach experiments were imported into ImageJ. The 10 pre-bleach frames were averaged and used as a baseline to normalize all post-bleach frames. Recovery curves of fluorescence intensity within the bleached region of the PM were determined using an ROI with a diameter of 1.54 μm over the bleached spot for all frames. The MF was determined by the maximal projected value, Y_{MAX}, of the recovery curves.

D_{FRAP} was determined using the segmented line tool in ImageJ to trace the bleached region across the PM and fluorescence intensity recorded in the normalized image stack for 5–20 frames (1 frame/second) using the 'record profile' macro. Total cellular fluorescence was adjusted for experimental photobleaching. The normalized and adjusted profiles were analyzed in Prism (GraphPad Software) and fitted independently with the Gaussian function: $F(x)=1–Bxe–[(x–c)^2/r^2]$ where F is the normalized fluorescence intensity, c is the centre of the bleached profile (of distance x, in μm), B is the depth of the Gaussian profile and r is the Gaussian radius at e^{-1}. The values of r^2 were plotted against time (goodness of fit, $R^2>0.9$) and the gradient was proportional to D_{FRAP}, obtained from: $r^2=4Dt+r_0^2$, where t is time in seconds.

FCS

Cells were plated onto poly-L-lysine coated eight-well chambered coverglasses (Nunc Nalgene), and equilibrated to room temperature to minimize artefacts from temperature-induced PM fluctuations, before FCS measurements were taken on a Zeiss LSM510 ConfoCor 3 inverted confocal microscope using a 40× c-Apochromat 1.2 NA water-immersion objective. The confocal volume was calibrated on the day of each experiment using 20 nM Rhodamine 6G, the confocal volume was positioned over the cell nucleus, (488 nm excitation, with emission detected through a LP505 emission filter) and the focal plane was positioned precisely on the upper PM peak, using an intensity z-scan. Data were collected using 488 nm excitation with emission collected through a BP505-610IR emission filter, for 1×20 seconds at a laser intensity of 0.08 kW/cm^2 following a 10-second pre-bleach at the same laser power. Data were analyzed using Zeiss AIM4.2 software. Autocorrelation data was fitted using non-linear regression to a two-component, two-dimensional diffusion model, incorporating a pre-exponential component to account for fast GFP blinking. The first of these two-dimensional components was accounted for by photophysics of the GFP, and the second was representative of AC8 diffusion. The confocal volume dimensions were calculated from a calibration FCS read using 20 nM Rhodamine 6G, as previously described (Briddon et al., 2004). D_{FCS} were calculated using the equation $D=\omega_0^2/4.\tau_D$, where ω_0 is the radius of the beam waist of the detection volume and τ_D is the average dwell time of the AC8 in the volume as determined by autocorrelation analysis. Particle number was calculated directly from the fractional contribution of the GFP diffusing component to the total particle number as determined by autocorrelation. This was subsequently expressed in particles per μm^2 (Nμ/m^2), by normalizing to $\pi\omega_0^2$. Photon counting histogram (PCH) data were fitted to a single component curve using a bin time of 100 μseconds, with a first-order correction fixed to that obtained for a calibration read using 20 nM Rhodamine 6G. Careful examination of the data led to the exclusion of eight diffusion outliers (out of 50 recordings) for MβCD-treated cells, which were up to 240 times faster than the average. These very fast diffusions might represent the photophysical blinking of the GFP, as they were in the correct time range.

Western blot analysis

GFP-tagged AC8-based proteins were resolved using a 6% (w/v) SDS-polyacrylamide gel, before being transferred onto a nitrocellulose membrane and electrophoresed for 90 minutes at 300 mA. Membranes were blocked in TBS-T (20 mM Tris, pH 7.5, 150 mM NaCl and 0.05% (v/v) Tween 20) containing 5% (w/v) non-fat dry milk (16 hours at 4℃). Membranes were rinsed in TBS-T before incubating with anti-GFP antibody (2 μg/ml) for 1 hour and then rinsed again. Membranes were incubated with goat anti-mouse IgG conjugated to horseradish peroxidase (100 ng/ml) for 1 hour before rinsing in TBS-T then TBS (20 mM Tris, pH 7.5 and 150 mM NaCl). Membranes were visualized using ECL Plus reagent.

Statistics

Statistical significance of colocalisation, $Ratio_{PM/Cyt}$, cAMP accumulation and Epac2-camps experiments were determined using Student's t-tests with Welch's correction. Densitometry, FRAP and FCS data were analysed by one-way ANOVA with Neuman–Keuls multiple comparison tests. In each case, the number in brackets (n) refers to the number of cells measured in at least three separate experiments, or the number of times the experiment was repeated, as appropriate. Data are presented as the means ± s.e.m.; n.s., not significant; asterisks: $*P<0.05$, $**P<0.01$ and $***P<0.001$ in comparison to untreated control or otherwise indicated.

Acknowledgements

We thank Sebastian Wachten for assistance with molecular biology, and D. Willoughby and N. Masada for helpful comments on the manuscript.

Funding

This work was supported by a program grant from the European Commission [grant number 037189] led by Enno Klussmann; the Wellcome Trust [grant number RG31760 to D.M.F.C.]; and a Royal Society Wolfson Research Fellowship to D.M.F.C. Deposited in PMC for release after 6 months.

Supplementary material available online at
http://jcs.biologists.org/lookup/suppl/doi:10.1242/jcs.091090/-/DC1

References

Bacskai, B. J., Hochner, B., Mahaut-Smith, M., Adams, S. R., Kaang, B. K., Kandel, E. R. and Tsien, R. Y. (1993). Spatially resolved dynamics of cAMP and protein kinase A subunits in Aplysia sensory neurons. *Science* **260**, 222-226.

Bauman, A. L., Soughayer, J., Nguyen, B. T., Willoughby, D., Carnegie, G. K., Wong, W., Hoshi, N., Langeberg, L. K., Cooper, D. M. F., Dessauer, C. W. et al.

(2006). Dynamic regulation of cAMP synthesis through anchored PKA-adenylyl cyclase V/VI complexes. *Mol. Cell* **23**, 925-931.

Boyajian, C. L., Garritsen, A. and Cooper, D. M. F. (1991). Bradykinin stimulates Ca^{2+} mobilization in NCB-20 cells leading to direct inhibition of adenylylcyclase. A novel mechanism for inhibition of cAMP production. *J. Biol. Chem.* **266**, 4995-5003.

Briddon, S. J., Middleton, R. J., Cordeaux, Y., Flavin, F. M., Weinstein, J. A., George, M. W., Kellam, B. and Hill, S. J. (2004). Quantitative analysis of the formation and diffusion of A1-adenosine receptor-antagonist complexes in single living cells. *Proc. Natl. Acad. Sci. USA* **101**, 4673-4678.

Brown, D. A. and London, E. (1998). Functions of lipid rafts in biological membranes. *Ann. Rev. Cell Dev. Biol.* **14**, 111-136.

Brown, D. A. and London, E. (2000). Structure and function of sphingolipid- and cholesterol-rich membrane rafts. *J. Biol. Chem*. **275**, 17221-17224.

Buxton, I. L. and Brunton, L. L. (1983). Compartments of cyclic AMP and protein kinase in mammalian cardiomyocytes. *J. Biol. Chem.* **258**, 10233-10239.

Cha, B., Kenworthy, A., Murtazina, R. and Donowitz, M. (2004). The lateral mobility of NHE3 on the apical membrane of renal epithelial OK cells is limited by the PDZ domain proteins NHERF1/2, but is dependent on an intact actin cytoskeleton as determined by FRAP. *J Cell Sci*. **117**, 3353-3365.

Cheng, K. T., Liu, X., Ong, H. L., Swaim, W. and Ambudkar, I. S. (2011). Local Ca^{2+} entry via Orai1 regulates plasma membrane recruitment of TRPC1 and controls cytosolic Ca^{2+} signals required for specific cell functions. *PLoS Biol.* **9**, e1001025.

Chichili, G. R. and Rodgers, W. (2007). Clustering of membrane raft proteins by the actin cytoskeleton. *J. Biol. Chem*. **282**, 36682-36691.

Chou, J. L., Huang, C. L., Lai, H. L., Hung, A. C., Chien, C. L., Kao, Y. Y. and Chern, Y. (2004). Regulation of type VI adenylyl cyclase by Snapin, a SNAP25-binding protein. *J. Biol. Chem*. **279**, 46271-46279.

Contreras, F. X., Villar, A. V., Alonso, A., Kolesnick, R. N. and Goni, F. M. (2003). Sphingomyelinase activity causes transbilayer lipid translocation in model and cell membranes. *J. Biol. Chem*. **278**, 37169-37174.

Cooper, D. M. F. and Crossthwaite, A. J. (2006). Higher-order organization and regulation of adenylyl cyclases. *Trends Pharmacol. Sci.* **27**, 426-431.

Cristofanilli, M., Mizuno, F. and Akopian, A. (2007). Disruption of actin cytoskeleton causes internalization of Ca(v)1.3 (alpha 1D) L-type calcium channels in salamander retinal neurons. *Mol. Vis*. **13**, 1496-1507.

Crossthwaite, A. J., Ciruela, A., Rayner, T. F. and Cooper, D. M. F. (2006). A direct interaction between the N terminus of adenylyl cyclase AC8 and the catalytic subunit of protein phosphatase 2A. *Mol. Pharmacol*. **69**, 608-617.

Dell'Acqua, M. L., Smith, K. E., Gorski, J. A., Horne, E. A., Gibson, E. S. and Gomez, L. L. (2006). Regulation of neuronal PKA signalling through AKAP targeting dynamics. *Eur. J. Cell Biol.* **85**, 627-633.

dos Remedios, C. G., Chhabra, D., Kekic, M., Dedova, I. V., Tsubakihara, M., Berry, D. A. and Nosworthy, N. J. (2003). Actin binding proteins: regulation of cytoskeletal microfilaments. *Physiol. Rev*. **83**, 433-473.

Edidin, M. (1992). Patches, posts and fences: proteins and plasma membrane domains. *Trends Cell Biol.* **2**, 376-380.

Efendiev, R., Samelson, B. K., Nguyen, B. T., Phatarpekar, P. V., Baameur, F., Scott, J. D. and Dessauer, C. W. (2010). AKAP79 interacts with multiple adenylyl cyclase (AC) isoforms and scaffolds AC5 and -6 to alpha-amino-3-hydroxyl-5-methyl-4-isoxazole-propionate (AMPA) receptors. *J. Biol. Chem*. **285**, 14450-14458.

Enserink, J. M., Christensen, A. E., de Rooij, J., van Triest, M., Schwede, F., Genieser, H. G., Døskeland, S. O., Blank, J. L. and Bos, J. L. (2002). A novel Epac-specific cAMP analogue demonstrates independent regulation of Rap1 and ERK. *Nat. Cell Biol.* **4**, 901-906.

Fagan, K. A., Mahey, R. and Cooper, D. M. F. (1996). Functional co-localization of transfected Ca^{2+}-stimulable adenylyl cyclases with capacitative Ca^{2+} entry sites. *J. Biol. Chem.* **271**, 12438-12444.

Gruenberg, J. (2001). The endocytic pathway: a mosaic of domains. *Nat. Rev. Mol. Cell Biol*. **2**, 721-730.

Gu, C. and Cooper, D. M. F. (1999). Calmodulin-binding sites on adenylyl cyclase type VIII. *J. Biol. Chem.* **274**, 8012-8021.

Haggie, P. M., Stanton, B. A. and Verkman, A. S. (2004). Increased diffusional mobility of CFTR at the plasma membrane after deletion of its C-terminal PDZ binding motif. *J. Biol. Chem*. **279**, 5494-5500.

Halls, M. L. and Cooper, D. M. F. (2010). Sub-picomolar relaxin signaling by a pre-assembled RXFP1, AKAP-79, AC2, β-arrestin 2, PDE4D3 complex. *EMBO J.* **29**, 2772-2787.

Hammond, G. R., Sim, Y., Lagnado, L. and Irvine, R. F. (2009). Reversible binding and rapid diffusion of proteins in complex with inositol lipids serves to coordinate free movement with spatial information. *J. Cell Biol*. **184**, 297-308.

Hancock, J. F. and Parton, R. G. (2005). Ras plasma membrane signalling platforms. *Biochem. J*. **389**, 1-11.

Hansen, G. H., Niels-Christiansen, L. L., Thorsen, E., Immerdal, L. and Danielsen, E. M. (2000). Cholesterol depletion of enterocytes. Effect on the Golgi complex and apical membrane trafficking. *J. Biol. Chem*. **275**, 5136-5142.

Haustein, E. and Schwille, P. (2004). Single-molecule spectroscopic methods. *Curr. Opin. Struct. Biol*. **14**, 531-540.

Head, B. P., Patel, H. H., Roth, D. M., Murray, F., Swaney, J. S., Niesman, I. R., Farquhar, M. G. and Insel, P. A. (2006). Microtubules and actin microfilaments regulate lipid raft/caveolae localization of adenylyl cyclase signaling components. *J. Biol. Chem*. **281**, 26391-26399.

Howe, A. K. (2004). Regulation of actin-based cell migration by cAMP/PKA. *Biochim. Biophys. Acta* **1692**, 159-174.

Iancu, R. V., Ramamurthy, G. and Harvey, R. D. (2008). Spatial and temporal aspects of cAMP signalling in cardiac myocytes. *Clin. Exp. Pharmacol. Physiol*. **35**, 1343-1348.

Ilangumaran, S. and Hoessli, D. C. (1998). Effects of cholesterol depletion by cyclodextrin on the sphingolipid microdomains of the plasma membrane. *Biochem. J.* **335**, 433-440.

Jurevicius, J. and Fischmeister, R. (1996). cAMP compartmentation is responsible for a local activation of cardiac Ca^{2+} channels by beta-adrenergic agonists. *Proc. Natl. Acad. Sci. USA* **93**, 295-299.

Kenworthy, A. K., Nichols, B. J., Remmert, C. L., Hendrix, G. M., Kumar, M., Zimmerberg, J. and Lippincott-Schwartz, J. (2004). Dynamics of putative raft-associated proteins at the cell surface. *J. Cell Biol.* **165**, 735-746.

Kim, S. A., Heinze, K. G. and Schwille, P. (2007). Fluorescence correlation spectroscopy in living cells. *Nat. Methods* **4**, 963-973.

Kusumi, A., Nakada, C., Ritchie, K., Murase, K., Suzuki, K., Murakoshi, H., Kasai, R. S., Kondo, J. and Fujiwara, T. (2005). Paradigm shift of the plasma membrane concept from the two-dimensional continuum fluid to the partitioned fluid: high-speed single-molecule tracking of membrane molecules. *Annu. Rev. Biophys. Biomol. Struct*. **34**, 351-378.

Langhorst, M. F., Solis, G. P., Hannbeck, S., Plattner, H. and Stuermer, C. A. (2007). Linking membrane microdomains to the cytoskeleton: regulation of the lateral mobility of reggie-1/flotillin-2 by interaction with actin. *FEBS Lett*. **581**, 4697-4703.

Li, H. and Papadopoulos, V. (1998). Peripheral-type benzodiazepine receptor function in cholesterol transport. Identification of a putative cholesterol recognition/interaction amino acid sequence and consensus pattern. *Endocrinology* **139**, 4991-4997.

Lingwood, D., Ries, J., Schwille, P. and Simons, K. (2008). Plasma membranes are poised for activation of raft phase coalescence at physiological temperature. *Proc. Natl. Acad. Sci. USA* **105**, 10005-10010.

Lynch, M. J., Baillie, G. S. and Houslay, M. D. (2007). cAMP-specific phosphodiesterase-4D5 (PDE4D5) provides a paradigm for understanding the unique non-redundant roles that PDE4 isoforms play in shaping compartmentalized cAMP cell signalling. *Biochem. Soc. Trans*. **35**, 938-941.

Maciver, S. K. and Hussey, P. J. (2002). The ADF/cofilin family: actin-remodeling proteins. *Genome Biol.* **3**, reviews 3007.

Martin, A. C., Willoughby, D., Ciruela, A., Ayling, L. J., Pagano, M., Wachten, S., Tengholm, A. and Cooper, D. M. F. (2009). Capacitative Ca^{2+} entry via Orai1 and stromal interacting molecule 1 (STIM1) regulates adenylyl cyclase type 8. *Mol. Pharmacol*. **75**, 830-842.

Nadella, K. S., Saji, M., Jacob, N. K., Pavel, E., Ringel, M. D. and Kirschner, L. S. (2009). Regulation of actin function by protein kinase A-mediated phosphorylation of Limk1. *EMBO Rep*. **10**, 599-605.

Nakahashi, Y., Nelson, E., Fagan, K. A., Gonzales, E., Guillou, J. L. and Cooper, D. M. F. (1997). Construction of a full-length Ca^{2+}-sensitive adenylyl cyclase/aequorin chimera. *J. Biol. Chem.* **272**, 18093-18097.

Nikolaev, V. O., Bunemann, M., Hein, L., Hannawacker, A. and Lohse, M. J. (2004). Novel single chain cAMP sensors for receptor-induced signal propagation. *J. Biol. Chem*. **279**, 37215-37218.

Nikolaev, V. O., Bunemann, M., Schmitteckert, E., Lohse, M. J. and Engelhardt, S. (2006). Cyclic AMP imaging in adult cardiac myocytes reveals far-reaching beta1-adrenergic but locally confined beta2-adrenergic receptor-mediated signaling. *Circ. Res*. **99**, 1084-1091.

Nishimura, S. Y., Vrljic, M., Klein, L. O., McConnell, H. M. and Moerner, W. E. (2006). Cholesterol depletion induces solid-like regions in the plasma membrane. *Biophys. J*. **90**, 927-938.

Oancea, E., Teruel, M. N., Quest, A. F. and Meyer, T. (1998). Green fluorescent protein (GFP)-tagged cysteine-rich domains from protein kinase C as fluorescent indicators for diacylglycerol signaling in living cells. *J. Cell Biol*. **140**, 485-498.

O'Connell, K. M., Rolig, A. S., Whitesell, J. D. and Tamkun, M. M. (2006). Kv2.1 potassium channels are retained within dynamic cell surface microdomains that are defined by a perimeter fence. *J. Neurosci*. **26**, 9609-9618.

Pagano, M., Clynes, M. A., Masada, N., Ciruela, A., Ayling, L. J., Wachten, S. and Cooper, D. M. F. (2009). Insights into the residence in lipid rafts of adenylyl cyclase AC8 and its regulation by capacitative calcium entry. *Am. J. Physiol. Cell Physiol*. **296**, C607-C619.

Paller, M. S. (1994). Lateral mobility of Na,K-ATPase and membrane lipids in renal cells. Importance of cytoskeletal integrity. *J. Membr. Biol*. **142**, 127-135.

Pani, B., Ong, H. L., Liu, X., Rauser, K., Ambudkar, I. S. and Singh, B. B. (2008). Lipid rafts determine clustering of STIM1 in ER-plasma membrane junctions and regulation of SOCE. *J. Biol. Chem*. **20**, 17333-17340.

Parekh, A. B. and Putney, J. W. (2005). Store-operated calcium channels. *Physiol. Rev.* **85**, 757-810.

Park, W. S., Heo, W. D., Whalen, J. H., O'Rourke, N. A., Bryan, H. M., Meyer, T. and Teruel, M. N. (2008). Comprehensive identification of PIP3-regulated PH domains from C. elegans to H. sapiens by model prediction and live imaging. *Mol. Cell* **30**, 381-392.

Popik, W. and Alce, T. M. (2004). CD4 receptor localized to non-raft membrane microdomains supports HIV-1 entry. Identification of a novel raft localization marker in CD4. *J. Biol. Chem*. **279**, 704-712.

Pucadyil, T. J., Mukherjee, S. and Chattopadhyay, A. (2007). Organization and dynamics of NBD-labeled lipids in membranes analyzed by fluorescence recovery after photobleaching. *J. Phys. Chem. B* **111**, 1975-1983.

Rich, T. C., Fagan, K. A., Nakata, H., Schaack, J., Cooper, D. M. F. and Karpen, J. W. (2000). Cyclic nucleotide-gated channels colocalize with adenylyl cyclase in regions of restricted cAMP diffusion. *J. Gen. Physiol.* **116**, 147-161.

Rodgers, W. and Zavzavadjian, J. (2001). Glycolipid-enriched membrane domains are assembled into membrane patches by associating with the actin cytoskeleton. *Exp. Cell Res*. **267**, 173-183.

Rossin, A., Kral, R., Lounnas, N., Chakrabandhu, K., Mailfert, S., Marguet, D. and Hueber, A. O. (2010). Identification of a lysine-rich region of Fas as a raft nanodomain targeting signal necessary for Fas-mediated cell death. *Exp. Cell Res*. **316**, 1513-1522.

Ruppelt, A., Mosenden, R., Gronholm, M., Aandahl, E. M., Tobin, D., Carlson, C. R., Abrahamsen, H., Herberg, F. W., Carpen, O. and Tasken, K. (2007). Inhibition of T cell activation by cyclic adenosine 5′-monophosphate requires lipid raft targeting of protein kinase A type I by the A-kinase anchoring protein ezrin. *J. Immunol*. **179**, 5159-5168.

Sako, Y. and Kusumi, A. (1994). Compartmentalized structure of the plasma membrane for receptor movements as revealed by a nanometer-level motion analysis. *J. Cell Biol*. **125**, 1251-1264.

Salgado, A., Ordaz, B., Sampieri, A., Zepeda, A., Glazebrook, P., Kunze, D. and Vaca, L. (2008). Regulation of the cellular localization and function of human transient receptor potential channel 1 by other means of the TRPC family. *Cell Calcium* **43**, 375-387.

Schroeder, F., Woodford, J. K., Kavecansky, J., Wood, W. G. and Joiner, C. (1995). Cholesterol domains in biological membranes. *Mol. Membr. Biol*. **12**, 113-119.

Schubert, T. and Akopian, A. (2004). Actin filaments regulate voltage-gated ion channels in salamander retinal ganglion cells. *Neuroscience* **125**, 583-590.

Schwille, P. (2001). Fluorescence correlation spectroscopy and its potential for intracellular applications. *Cell Biochem. Biophys*. **34**, 383-408.

Shvartsman, D. E., Gutman, O., Tietz, A. and Henis, Y. I. (2006). Cyclodextrins but not compactin inhibit the lateral diffucion of membrane proteins independent of cholesterol. *Traffic* **7**, 917-926.

Simpson, R. E., Ciruela, A. and Cooper, D. M. F. (2006). The role of calmodulin recruitment in Ca^{2+}-stimulation of adenylyl cyclase type 8. *J. Biol. Chem*. **281**, 17379-17389.

Smith, K. E., Gu, C., Fagan, K. A., Hu, B. and Cooper, D. M. F. (2002). Residence of adenylyl cyclase type 8 in caveolae is necessary but not sufficient for regulation by capacitative Ca^{2+} entry. *J. Biol. Chem.* **277**, 6025-6031.

Stahlhut, M. and van Deurs, B. (2000). Identification of filamin as a novel ligand for caveolin-1: evidence for the organization of caveolin-1-associated membrane domains by the actin cytoskeleton. *Mol. Biol. Cell* **11**, 325-337.

Staneva, G., Momchilova, A., Wolf, C., Quinn, P. J. and Koumanov, K. (2009). Membrane microdomains: role of ceramides in the maintenance of their structure and functions. *Biochim. Biophys. Acta* **1788**, 666-675.

Suzuki, K., Ritchie, K., Kajikawa, E., Fujiwara, T. and Kusumi, A. (2005). Rapid hop diffusion of a G-protein-coupled receptor in the plasma membrane as revealed by single-molecule techniques. *Biophys. J*. **88**, 3659-3680.

Tamkun, M. M., O'Connell, M. and Rolig, A. S. (2007). A cytoskeletal-based perimeter fence selectively corrals a sub-population of cell surface Kv2.1 channels. *J. Cell Sci*. **120**, 2413-2423.

Tesmer, J. J., Sunahara, R. K., Johnson, R. A., Gosselin, G., Gilman, A. and Sprang, S. R. (1999). Two-metal-Ion catalysis in adenylyl cyclase. *Science* **285**, 756-760.

Tomishige, M., Sako, Y. and Kusumi, A. (1998). Regulation of the lateral diffusion of band 3 in erythrocyte membranes by the membrane skeleton. *J. Cell Biol.* **142**, 989-1000.

Umemura, M., Vrljic, M., Nishimura, S. Y., Fujiwara, T. K., Suzuki, K. G. and Kusumi, A. (2008). Both MHC class II and its GPI-anchored form undergo hop diffusion as observed by single-molecule tracking. *Biophys. J.* **95**, 435-450.

Wachten, S., Masada, N., Ayling, L. J., Ciruela, A., Nikolaev, V. O., Lohse, M. J. and Cooper, D. M. F. (2010). Distinct pools of cAMP centre on different isoforms of adenylyl cyclase in pituitary-derived GH3B6 cells. *J. Cell Sci*. **123**, 95-106.

Willoughby, D. and Cooper, D. M. F. (2007). Organization and Ca^{2+} regulation of adenylyl cyclases in cAMP microdomains. *Physiol. Rev*. **87**, 965-1010.

Willoughby, D., Masada, N., Crossthwaite, A. J., Ciruela, A. and Cooper, D. M. F. (2005). Localized Na^{+}/H^{+} exchanger 1 expression protects Ca^{2+}-regulated adenylyl cyclases from changes in intracellular pH. *J. Biol. Chem*. **280**, 30864-30872.

Willoughby, D., Wong, W., Schaack, J., Scott, J. D. and Cooper, D. M. F. (2006). An anchored PKA and PDE4 complex regulates subplasmalemmal cAMP dynamics. *EMBO J*. **25**, 2051-2061.

Willoughby, D., Wachten, S., Masada, N. and Cooper, D. M. F. (2010a). Direct demonstration of discrete Ca^{2+} microdomains associated with different isoforms of adenylyl cyclase. *J. Cell Sci*. **123**, 107-117.

Willoughby, D., Masada, N., Wachten, S., Pagano, M., Halls, M., Everett, K. L., Ciruela, A. and Cooper, D. M. F. (2010b). A-kinase anchoring protein 79/150 interacts with adenylyl cyclase type 8 and regulates Ca^{2+}-dependent cAMP synthesis in pancreatic and neuronal systems. *J. Biol. Chem*. **285**, 20328-20342.

Zaccolo, M. and Pozzan, T. (2002). Discrete microdomains with high concentration of cAMP in stimulated rat neonatal cardiac myocytes. *Science* **295**, 1711-1715.

Zidovetzki, R. and Levitan, I. (2007). Use of cyclodextrin to manipulate plasma membrane cholesterol content: evidence, misconceptions and control strategies. *Biochim. Biophys. Acta* **1768**, 1311-1324.